INSTITUTE OF PHYSICS PUBLISHING REPORTS ON PROGRESS IN PHYSICS

Rep. Prog. Phys. **64** (2001) 777–814 PII: S0034-4885(01)18686-0

The structure of the surface of pure liquids

Jeffrey Penfold

ISIS Facility, Rutherford Appleton Laboratory, CLRC, Chilton, Didcot, OXON, UK

Received 21 December 2000, in final form 4 May 2001
Published 26 June 2001
Online at stacks.iop.org/RoPP/64/777

Abstract

This paper reviews the progress in the study of the structure of the surface of pure liquids made in the last 10–20 years. This area of research has benefited enormously in recent years from developments in experimental techniques (especially x-ray scattering methods based on third-generation synchrotron sources, and advanced optical techniques) and theory (particularly computer simulation and density functional theory). The review is predominantly experimentally based, and focuses very much on some recent exciting new results and developments. Specific systems or phenomena that are discussed are molecular ordering and orientation at the surface, atomic-scale layering at liquid metal surfaces, surface freezing in liquid alkanes and alcohols, surface melting and pre-melting at the water surface, thermal roughness (capillary waves) in simple liquids, and visco-elastic surface waves. Both the liquid–vapour and liquid–solid interfaces are considered. Some details of the principal experimental techniques exploited, x-ray reflectivity, diffuse x-ray scattering, grazing incidence x-ray diffraction, ellipsometry, light scattering, will be given, The experimental developments have gone very much in conjunction with substantial theoretical advances, and the principal theoretical concepts will be briefly discussed.

Contents

1. Introduction

Interest in the structure of the surface of simple liquids has a long and distinguished tradition in physics. The focus of this research has always been to understand the equilibrium thermodynamic properties, such as surface tension, in terms of the microscopic structure. Although considerable progress has been made in understanding the equilibrium bulk properties of uniform fluids, the surface or interface is less well understood. The introduction of a non-uniform or inhomogeneous distribution, as presented by an interface, poses both theoretical and experimental challenges. A detailed theory of the statistical mechanics of non-uniform fluids is essential for the understanding of the structure of the liquid–vapour interface, surface tension, contact angle, wetting, and other interfacial phenomena. The pioneering work of van der Waals [1] and Lord Rayleigh [2] has provided the basis for much of the subsequent theoretical developments.

The late 1970s and early 1980s saw a great deal of both theoretical and experimental effort in this area. Much of that theoretical progress has been encapsulated in some excellent specialist books, which include *The Molecular Theory of Capillarity* by Rowlinson and Widom [3], *The Statistical Mechanics of the Liquid Surface* by Croxton [4], and some key reviews (see, for example, [5]). The field, both theory and experiment, was comprehensively reviewed in the proceedings of the Faraday Discussion on *The Structure of the Interfacial Region* in 1981 [6], and many of those contributions remain as classical contributions to the field. A similar compilation was also made by Croxton [7] in 1986. Although this earlier pioneering work will provide a starting point, the more recent developments will be the main focus of the review.

In recent years there has been much resurgence in activity and interest in this field. In part this may be due to the increasing importance and technological relevance of surfaces and interfaces, especially in the context of 'complex fluids'. The study of complex fluids is an area involving the behaviour of polymers, surfactants, complex mixtures and complex mesophases at interfaces (see, for example, [8]), and is beyond the scope of this review. This is only part of the picture, and the surface of simple liquids remains an important subject in its own right. The study of the surface of liquids has always been an experimental challenge as far back as the pioneering work of Jamin [8], Rayleigh [2] and others. However, much of the renewed activity arises from recent developments in experimental techniques (especially surface-sensitive x-ray scattering methods based on third-generation synchrotron radiation sources and advanced optical techniques), and theory (particularly density functional theory and the greater computing power available for meaningful simulations). The review will be heavily biased towards the recent experimental results and developments. However, these recent experimental developments go hand in hand with developments in the theory. Sufficient theory to understand the recent experimental results and to provide the necessary background will be included. The recent developments in experimental techniques are of particular importance, and details of the principal experimental techniques used will be described. These include principally x-ray reflectivity, diffuse surface x-ray scattering, grazing incidence x-ray diffraction and scattering, and the optical techniques of ellipsometry, surface quasi-elastic scattering, sum frequency and second-harmonic generation. The specific surface phenomena that will be discussed include molecular ordering and orientation at the surface, atomic-scale layering at the liquid metal surface, surface freezing and melting in liquid alkanes and alcohols, freezing and pre-melting at the water interface, capillary waves (CW) and visco-elastic surface waves. Both the liquid–vapour and the liquid–solid interfaces will be considered. Particular systems that will be discussed are the liquid–vapour interfaces of the metals mercury, sodium, potassium, caesium, rubidium, gallium and indium, simple liquids such as water, molecular fluids which includes a range of alkanes and alcohols, and the liquid–vapour interface of helium

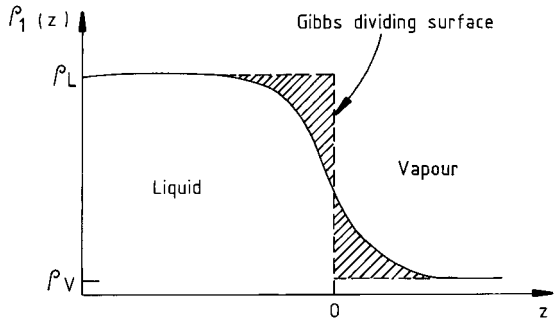

Figure 1. Schematic representation of the liquid–vapour interface, showing the variation in density $\rho_1(z)$ with z, from the liquid density ρ_L to the vapour density ρ_V, and illustrating the concept of the Gibbs dividing surface.

and argon. The study of complex mixtures and adsorption phenomena will not be included. The study of wetting is a rich field of activity, but too extensive to include here, and warrants a review of its own.

2. Theoretical background

As with bulk liquids, the ultimate objective of theoretical treatments of the liquid/vapour interface is to relate the thermodynamic properties (such as surface tension and surface free energy) and microscopic structure to the inter-molecular potential. The sharp density discontinuity separating the two homogeneous co-existing liquid and vapour phases imposes an inhomogeneity which further complicates the application of statistical mechanics. In bulk fluids it is the two-body distribution function $g_2(r_{12})$ which is of central importance and experimentally accessible. At the interface or surface, both the one- and two-particle density functions $\rho_1(r_1)$ and $\rho_2(r_1, r_2)$ are of importance. A concept that was central to the development of the statistical mechanical approach was the 'dividing surface' introduced by Gibbs [9] (see figure 1).

The Gibbs excess of a quantity is the excess of the real two-phase system over a hypothetical reference system in which the bulk properties remain constant up to the dividing surface separating the two bulk phases. The Gibbs dividing surface was chosen such that

$$\int_{-\infty}^{0} [\rho_1(z) - \rho_L]\,\mathrm{d}z = \int_{0}^{\infty} [\rho_1(z) - \rho_v]\,\mathrm{d}z \tag{1}$$

where ρ_L, ρ_V are the liquid and vapour number densities.

The inhomogeneity in the local density implies that the one- and two-particle distribution functions are anisotropic,

$$\rho_2(z_1, r_{12}) = \rho_1(z_1)\,\rho_1(z_2)\,g(z_1, r_{12})\,. \tag{2}$$

In direct analogy with the uniform fluid, finding an appropriate 'closure' relationship has been extensively discussed, and is suitably summarized by Croxton [4] and Evans [5]. In the early theoretical developments, such as the theories due to Kirkwood and Buff [10], and Fowler [11], isotropic bulk distribution functions were incorporated.

Density functional theory [5, 12] has been extensively applied, where the non-uniform equilibrium density profile minimizes the appropriate variational functional. The functional depends parametrically on the thermodynamic state of the system and on the microscopic

interactions present. Density functional theory is essentially a mean field treatment and perhaps the simplest and earliest manifestation was the approach of van der Waals [1], which is closely related to the Ornstein–Zernicke direct correlation function. In this case the simplest theory expands the free energy of the inhomogeneous fluid as a series of density gradients. Truncation at the square-gradient terms results in a theory of the same form as that of van der Waals. Widom [6] (and Evans [5]) both describe the theory of van der Waals and its relationship to more recent and sophisticated developments of density functional theory. Following Evans [5], in a simple homogeneous atomic fluid in the presence of a spatially varying external potential $V_{\text{ext}}(r)$, the Hamiltonian for N atoms has the form

$$\begin{aligned} H_N &= \sum_{i=1}^{N} \frac{P_i^2}{2m} + \Phi\,(r_1 \ldots r_N) + \sum_{i=1}^{N} V_{\text{ext}}\,(r_i) \\ &\equiv \text{KE} + \Phi + V_{\text{ext}}. \end{aligned} \tag{3}$$

P_i is the momentum of the ith atom, KE is the kinetic energy ($P^2/2m$) and the external potential couples to the microscopic particle density $\rho(r)$. From this the grand canonical ensemble can be determined, and the second functional derivative (with respect to the potential) gives rise to the density–density correlation function. This is in turn related to the familiar two-body distribution function $\rho_2(r_1, r_2)$. A second hierarchy of correlation functions, related to the direct correlation function $c(r)$, is generated from the density functional. Direct use of the same variational principle has been extended to inhomogeneous fluids and a range of interfacial problems.

It is well known that liquid surfaces are perturbed by long-wavelength fluctuations or correlations parallel to the surface, CWs, and whether they should be considered as part of the intrinsic interface or a perturbation has been extensively debated [5, 6]. These lateral correlations have a coherence length, ξ_0, that depends on the gravitational acceleration, g, the density difference of the two co-existing phases, $\Delta\rho$, and the surface tension, γ, such that

$$\xi_0 = \sqrt{(\gamma/g\Delta\rho)}. \tag{4}$$

Mean field theories, in which these long-range fluctuations are suppressed, yield an intrinsic interfacial structure; and early attempts to reconcile these interfacial structures with CW theory considered the CW as a perturbation on that intrinsic structure (see, for example, Percus, and Widom in [6]). Evans [5, 13] has discussed the limitations of this approach. However, Evans points out that the basic idea that the density profile is broadened by CW-like fluctuations is qualitatively correct, and this has formed the basis of much of the analysis of recent experimental data. In the CW model the transition from liquid to vapour is locally abrupt, but having fluctuations in height $h(x, y)$; and where $\sigma_{\text{cw}}^2 \equiv \left\langle h^2\,(x, y)\right\rangle_A$, the CW contribution to the interfacial width, the average over some area, A. The energy associated with non-uniform variations can be expressed in terms of a local energy density,

$$E = \frac{1}{2}\rho_{\text{m}} g h\,(x, y)^2 + \frac{1}{2}\gamma \left\{ \left[\frac{\partial h\,(x, y)}{\partial x} \right]^2 + \left[\frac{\partial h\,(x, y)}{\partial y} \right]^2 \right\} \tag{5}$$

where ρ_{m} is the fluid mass density. The ensemble average (from standard statistical mechanics) can be written as

$$\left\langle h^2(x, y)\right\rangle = \frac{k_{\text{B}}T}{4\pi^2\gamma} \int_{Aq} \frac{1}{q^2 + k_{\text{g}}^2}\, \mathrm{d}^2 q \tag{6}$$

where $A_q = 1/A$ is an area in the two-dimensional reciprocal space of the in-plane CW wavevectors, $k_{\text{g}}^2 = \frac{\rho m g}{\gamma}$, and q is the CW wavevector.

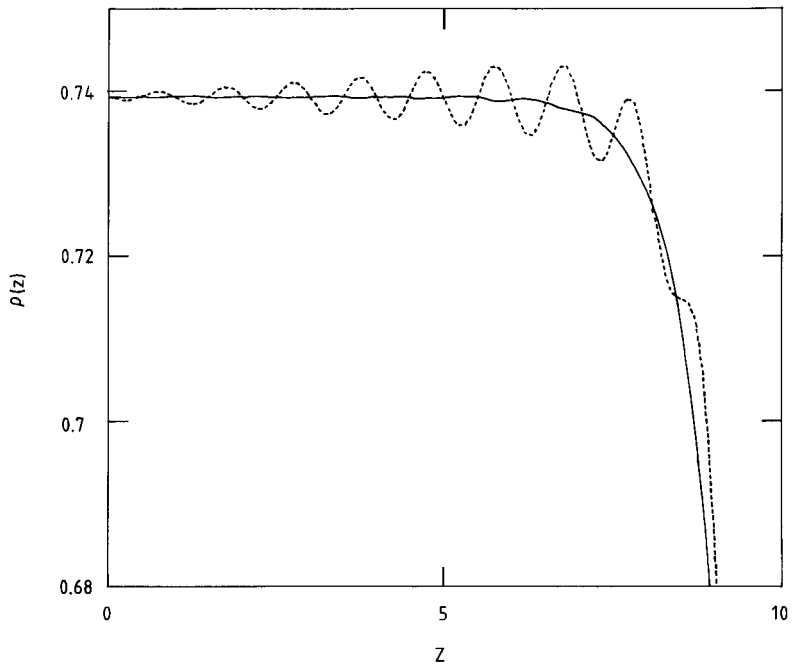

Figure 2. Liquid–vapour density profile, from WDA theory for a square-well fluid at $T/T_c = 0.64$. The dashed curve is the equilibrium profile, showing an oscillatory decay into the bulk liquid, and the solid curve is a smoothed curve (reproduced from [18]).

This leads to an expression for the broadening of the intrinsic interfacial width of the form

$$\sigma_{cw}^2 = \frac{kT}{4\pi\gamma} \ln\left(\frac{k_g^2 + q_{max}^2}{k_{0g}^2 + q_{min}^2}\right) \tag{7}$$

where q_{min}, q_{max} are the limits of the integrand in the derivation of equation (6) and will be discussed in more detail later in the review.

The most comprehensive and recent theoretical developments are by Dietrich and co-workers [14, 15]. Based on density functional theory for inhomogeneous liquids, they have derived an effective Hamiltonian of the gas–liquid interface, which takes into account the presence of long-range dispersion forces in the fluid and the smooth variation of the intrinsic profile.

The nature of the density profile at the free liquid surface, $\rho_1(z)$, has been the subject of much conjecture: whether the structure is monotonic (smooth) or oscillatory (layered), and involving both computer simulation and a number of different theoretical approaches. Osborn and Croxton [16, 17] solved the Born–Green–Yvon (BGY) equation to obtain the density profile for the free liquid surface for a Lennard-Jones fluid and, depending on the closure scheme used, were able to obtain both monotonic and oscillatory profiles. Evans [18] used density functional calculations for a square-well fluid to show that, near to its triple point, the interfacial profile is oscillatory (see figure 2).

At higher temperatures, approaching the critical point, the oscillations are damped and a pure exponential decay is obtained. Capillary wave fluctuations were found to reduce the amplitude of the oscillations. The structuring predicted is quite subtle, as the amplitude of the oscillations is about 2% of the bulk liquid density. This poses a severe experimental challenge, and will be discussed later. Dietrich [19] has discussed the structure of fluids induced by interfaces.

Gokelmann *et al* [20] used a weighted density functional theory and the Ornstein–Zernicke equation to obtain the structure of a hard-sphere fluid near a hard wall, and compared the results with computer simulation and that obtained from the inhomogeneous Percus–Yevick theory.

Consideration of the liquid–vapour interface of molecular and ionic fluids presents additional complexity, and molecular orientation and electrostatic forces have to be taken into account. This has resulted in a greater use of computer simulation compared with analytical theories. For example, it is now well established from Monte Carlo simulations that the structure of the liquid/vapour interface of simple metals is significantly different to that of dielectric liquids. Arising from the different forms of the potential energy function, simple metals show stratification, whereas dielectric liquids exhibit smooth monotonic decays. Although the study of the orientational order at the liquid–vapour interface by simulation or a variety of analytical methods is well advanced, there is a distinct lack of experimental techniques for probing such orientational order. However, there remains a strong motivation for developments in this area, as the orientational order in molecular fluids with non-spherical shapes and anisotropic pair potentials have both positional and orientational degrees of freedom. The interplay between such factors will give rise to rich interfacial phenomena, as manifested in their bulk properties.

Thompson *et al* [21–23] have used perturbation theory and molecular dynamics simulations to obtain the liquid–vapour interfacial density orientation profile $\rho(z, \omega)$ for homonuclear diatomic molecules, such as Cl_2, N_2, CO_2 and HCl. The inter-molecular potential consisted of a site–site Lennard-Jones term plus a quadrupole–quadrupole term. Without the quadrupole term molecules are found to prefer a perpendicular orientation on the liquid side of the interface, with a greater tendency to be parallel on the gas side. With the quadrupole term present there is a reduced tendency for the molecules to orient perpendicular on the liquid side, whereas a strong quadrupole predicts parallel orientation. The perturbation theory approach and simulation give similar results. In the simulations N_2 and Cl_2 were directly compared, and for N_2 no detectable orientational correlations were observed. Shing and Gubbins [24] showed that Monte Carlo simulations using a similar inter-molecular potential were in good agreement with the mean field and perturbation theory predictions. The mean field approach, using the low-density limit of density functional theory, is, however, limited to small dipolar potentials.

Dietrich *et al* [25–27] have used density functional theory in a more general way to determine the interfacial structure (and other properties) for molecular fluids in general and for Stockmayer fluids in particular. A Stockmayer fluid is a one-component fluid with a strong dipole and long-range van der Waals interactions. The approach developed by Dietrich *et al* can be used on a range of molecular fluids, including liquid crystals, with more general anisotropic molecular potential than just dipole–dipole interaction. Their calculations are in good agreement with published Monte Carlo simulations, and from systematic studies of the effects of temperature and the strength of the dipole, they have revealed power law and scaling behaviour.

Water is a molecular fluid, which presents a particular challenge. Croxton [28, 29] has used the density functional approach (through a variational minimization of the local free energy) to investigate the degree of molecular alignment in the interfacial region of water in the temperature range of 2–200 °C. The water molecule was represented as an axially symmetrical point dipole and quadrupole centred within a spherical Lennard-Jones potential. A degree of molecular orientation was found to extend over a range of tens of angstroms, compared with an interfacial width of order 3 molecular diameters. The preferred orientation was with the water's proton directed towards the vapour phase. The relative contributions of the different interactions (such as dipole–dipole) to the surface potential and surface tension were determined. However, the surface potential obtained was significantly larger than previous theoretical and experimental estimates.

Ionic fluids and especially liquid metals present a formidable theoretical challenge. Groh *et al* [30] have investigated the liquid/vapour interface of an ionic fluid for a restricted primitive model (RPM), using density functional theory based on correlation functions for the inhomogeneous fluid in the mean spherical approximation (MSA). In the RPM, the ions are modelled as hard spheres of equal and opposite charge, and the RPM is considered as a good model for the alkali halides. The ionic interfacial density profiles are identical for both species, and similar to simple atomic fluids. Specific predictions for the interfacial width and surface tension were made.

Liquid metal surfaces are even more complex, due to complications introduced by the consideration of the positive ion cores and the conduction electrons, the highly inhomogeneous and disordered nature of the system, and the presence of metal–nonmetal transitions. The simplest approach is the Jellium model, in which the discreet ions in a real liquid metal are smeared out into a uniform neutralizing background in which the interacting electrons move. This approach has been extensively applied to crystalline metal surfaces, and to the density profiles and surface tension of charged fluids [31]. Several different statistical mechanical approaches, using both density functional theory and perturbation theory, have yielded good predictions of surface tension and interfacial structure, and CW theory gives a good account of the temperature dependence of the interfacial width. Most of the theoretical approaches predict an oscillatory or stratified interfacial structure, as widely expected. This is due to the drastic variation in the effective interaction potential, which depends strongly on the conduction electron density, metal–nonmetal transitions, and Friedel oscillations in the electron density, which also induce oscillations in the ion density.

D'Evelyn and Rice [32–34] have performed Monte Carlo computer simulations, in which the atomic motion is described by an effective Hamiltonian for the ions, to predict the surface structure of sodium and cesium. They used a more sophisticated Monte Carlo algorithm than in previous studies, in which the effective ion–ion interaction is density and position dependent. The pseudo-atom Hamiltonian is described by evaluating the electronic free energy of the metal to second order in the electron–ion pseudo-potential. In the pseudo-potential formalism the interaction between atomic cores and conduction electrons is replaced by a weak effective interaction. The simulations reveal considerable structure at the liquid–vapour interface, in the form of stable oscillations extending several atomic layers into the bulk fluid. More recently, Chekmarev *et al* [35] have performed self-consistent quantum Monte Carlo simulations of the structure of the liquid–vapour interface of the alkali metals Na, K, Rb, and Cs, using a semi-empirical empty core model potential. The electronic and ion density profiles show similar oscillatory profiles, which resemble previous simulation studies using more sophisticated model potentials. The simplified approach was developed to complement more detailed descriptions, and to provide the opportunity for systematic studies. In their latest Monte Carlo study Chekmarev *et al* [36] have calculated the structure of the liquid–vapour interface of mercury, and have obtained good agreement with recent x-ray data (see section 7). The use of a non-local pseudo-potential in the self-consistent Monte Carlo simulations leads to a stratified longitudinal density distribution which accurately predicts the x-ray data.

3. Experimental techniques

The experimental techniques predominantly used to obtain structural information about liquid surfaces are based on optical and x-ray scattering techniques. Indeed, the use of optical reflectivity and scattering dates back to the pioneering work of Jamin [8], Rayleigh [2] and others. The surface sensitivity of optical methods has been enhanced by developments in ellipsometry [37–39], surface quasi-elastic scattering [40–43], and sum frequency and second-

harmonic generation [44, 45]. Although the principle behind the application of x-ray specular reflectivity to the study of surfaces is well established [46], it is only within the past few years, as a result of the advent of synchrotron x-ray sources, that the technique has developed into such a powerful tool for the study of liquid surfaces on an atomic scale [47–50]. The phenomenal fluxes available at the current generation of synchrotron sources has given rise to the extensive exploitation of x-ray off-specular scattering [51] to provide further complementary information about structural fluctuations. Although the x-ray and neutron reflectivity techniques are closely related, available neutron fluxes have limited its application in the study of pure liquid surfaces. However, the different neutron scattering amplitudes for deuterium and hydrogen provide a distinct advantage, using judicial chemical substitution, to manipulate the refractive index distribution, and this has been extensively and successfully applied to a range of organic systems [52, 53].

3.1. Optical techniques

Optical measurements, which provide information about some aspects of the structure of liquid surfaces, include reflectivity, ellipsometry and quasi-elastic scattering. Reflectivity and ellipsometry measurements involve interpretation in terms of an interfacial thickness and refractive index. The formulation of optical reflectivity in terms of Fresnel coefficients and refractive index differences is well established [54], and is suited to the characterization of thick surface layers. Much of the discussion in the literature has centred on the interpretation of the reflectivity in terms of surface roughness and a diffuse surface gradient [38, 39]. The reflection of polarized light at an interface depends on its state of polarization, and light polarized perpendicular to the plane of reflection (s-polarized) is reflected differently from light polarized in the plane of reflection (p-polarized). Optical reflectivity and ellipsometry measurements close to the Brewster angle provide enhanced sensitivity, and make the properties of thinner layers accessible. At the Brewster angle the reflectivity for a perfect (Fresnel) interface vanishes for p-polarization. Ellipsometry measures the phase of the reflected light and is able to distinguish between light reflected due to a deviation from the Brewster angle and from deviations from a Fresnel interface. Hence, the contribution to the reflectivity of a thin layer at the interface and interfacial roughness as small as a few angstroms is measurable. In a related technique, Brewster angle microscopy uses the sensitivity of the reflected intensity at the Brewster angle to make images of density variations or molecular orientations at the surface [55]. At the Brewster angle, for a transparent dielectric, $\mathrm{Re}\{r_\mathrm{p}/r_\mathrm{s}\} = 0$ (where r_p, r_s are the Fresnel reflection coefficients for s and p polarization at a sharp interface), and its coefficient of ellipticity, $\bar{\rho}$, is defined as

$$\bar{\rho} = \frac{\pi}{\lambda}\frac{(1+\varepsilon_\mathrm{w})^{\frac{1}{2}}}{(1-\varepsilon_\mathrm{w})}\eta \tag{8}$$

where ε_w is the relative permittivity of water; and η has two contributions, from the interfacial roughness, η_r, and the structure of the layer, η_s, given by,

$$\eta_\mathrm{r} = -\frac{3\,(1-\varepsilon_\mathrm{w})^2}{2\,(1+\varepsilon_\mathrm{w})}\sqrt{\frac{\pi kT}{6\gamma}} \tag{9}$$

and

$$\eta_\mathrm{s} = \int \frac{(\varepsilon\,(z)-1)\,(\varepsilon\,(z)-\varepsilon_\mathrm{w})}{\varepsilon\,(z)}\,\mathrm{d}z \tag{10}$$

where $\varepsilon(z)$ is the profile of relative permittivity normal to the surface. As η_r is proportional to the square of the amplitude of the roughness, ellipsometry is very sensitive to the small-scale ($q\lambda \gg 1$) Fourier components of roughness, and provides, for example, a good measure

of bending elastic modulus [39]. In spite of the enhanced sensitivity, ellipsometry has been applied predominantly to the study of liquid surfaces and mixtures as the critical point or critical de-mixing, where the length scales diverge, is approached [37, 38].

Application of the techniques developed for photon correlation spectroscopy [56] has stimulated the use of quasi-elastic surface light scattering from thermally excited CWs as a non-perturbative probe of the dynamics of liquid surfaces [40–43], providing information complementary to the static structural measurements. The thermally excited displacement, ζ, of a free liquid surface can be described by a set of Fourier surface modes of the form

$$\zeta\,(r,t) = \zeta_0 \exp\left(\mathrm{i}\,(qr + \omega t)\right). \tag{11}$$

The complex wave frequency, ω, is observed by light scattering at a fixed wavevector, q, where ω and q are related by the dispersion equation

$$\left(\omega + 2\nu q^2\right)^2 + gq + \frac{\gamma q^3}{\rho} = 4\nu^2 q^4 \left(q^2 + \frac{\omega}{\nu}\right)^{\frac{1}{2}} \tag{12}$$

where ν is the viscosity of the fluid, and the frequencies (ω) and damping constants (Γ) of these modes are obtained from an approximate solution to equation (12),

$$\omega^2 = \frac{\gamma q^3}{\rho} + gq \tag{13}$$

and

$$\Gamma = 2\nu q^2. \tag{14}$$

3.2. X-ray scattering (specular reflectivity and off-specular scattering)

The optical properties of x-rays (and neutrons), with wavelengths of a few angstroms, at surfaces and interfaces can be described by the same elementary laws of reflection and refraction as the optics of electromagnetic waves with wavelengths that are orders of magnitude larger [54]. Detailed treatment is given elsewhere: see, for example, [57, 58]. For x-rays, the refractive indices of media are slightly less than unity, and are given by

$$n = 1 - \delta + \mathrm{i}\beta \tag{15}$$

$$\delta = \frac{r_0 \lambda^2}{2\pi} N_\mathrm{a} \sum_i \frac{\rho_i}{A_i} Z_i. \tag{16}$$

The imaginary component arises when the medium is absorbing, $\beta = \mu\lambda/4\pi$, N_a is Avogadro's number, r_0 is the classical electron radius, λ the wavelength of the incident radiation, ρ_i the density of element i with atomic weight A_i, atomic number Z_i, and μ is the mass adsorption coefficient. The typical values of δ are $\sim 10^{-6}$, and so the refractive index is only slightly different from 1.0. This means that the critical glancing angles, θ_c, are small, $\sim 0.1^\circ/$Å, and this has implications for the instrumentation. For many materials (at x-ray wavelengths $\sim$1–2 Å) β is 10^2–10^3 smaller than δ, and so can frequently be ignored without introducing significant errors. This is not true for materials with high atomic numbers and for x-rays with larger wavelengths, and in such cases the imaginary component of the refractive index has to be included.

Although the elementary laws of optics apply, a convenient expression for the specular reflectivity arises from the Born approximation [47, 55],

$$\frac{R\,(q_z)}{R_\mathrm{F}\,(q_z)} \approx \left| \frac{1}{\rho_0} \int_{-\infty}^{\infty} \frac{\mathrm{d}\langle \rho\ (z)\rangle}{\mathrm{d}z} \exp\left(-\mathrm{i} q_z z\right) \right|^2 = \left|\Phi\,(q_z)\right| \tag{17}$$

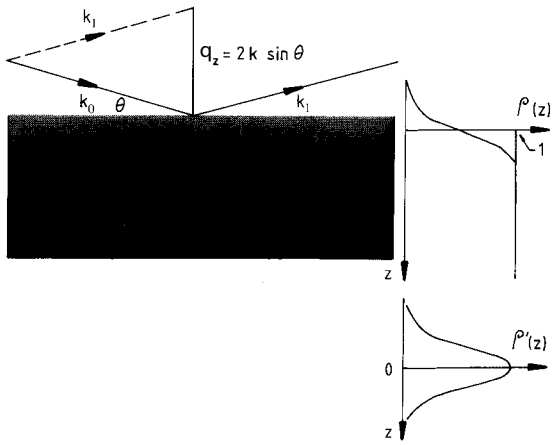

Figure 3. Scattering geometry for x-ray reflectivity.

where ρ_0 is the bulk density, q_z the wavevector transfer perpendicular to the surface ($q = k_0 - k_1$) (see figure 3), and $k = 2\pi/\lambda$.

$R_F(q_z)$ is the Fresnel reflectivity for a perfect bulk interface between two media,

$$R_F(q_z) = \left| \frac{\sin\theta - \sqrt{n^2 - \cos^2\theta}}{\sin\theta + \sqrt{n^2 - \cos^2\theta}} \right|^2. \tag{18}$$

For $\sin(\theta) \sim 0.0 \ll 1.0$, the reflectivity for s and p polarization are identical and

$$R_F(q_z) \approx \left(\frac{q_c}{2q_z}\right)^4 \tag{19}$$

where $q_c \approx \left(\frac{4\pi}{\lambda}\right)\theta_c$.

In most of the x-ray results discussed in this review, the data are presented in the form $R(q_z)/R_F(q_z)$ rather than as $R(q_z)$, so the $1/q_z^4$ Fresnel decay is removed. A typical x-ray reflectivity profile from the surface of pure water is shown in figure 4 [47].

The specular reflectivity provides, via the modulus squared of the Fourier transform of the density distribution, information about the refractive index (or its gradient) distribution at the interface. Interpretation of such data in terms of modelling, or in terms of different inversion schemes has been extensively discussed elsewhere [59–61].

In the simplest model, the liquid–vapour interface can be expressed as having a Gaussian form:

$$\frac{1}{\rho_0}\frac{d\rho(z)}{dz} = \frac{1}{\sqrt{2\pi\sigma^2}} \exp\left(-\frac{z^2}{2\sigma^2}\right) \tag{20}$$

and

$$\frac{R(q_z)}{R_F(q_z)} = \exp\left(-q_z^2\sigma^2\right). \tag{21}$$

As will be discussed later in more detail, when the contribution from CWs are taken into account the situation is more complex [60], and from earlier discussion (see equation (7)) the form is

$$\sigma^2 \equiv \sigma_0^2 + \left(\frac{k_B T}{4\pi\gamma}\right) \ln\left(q_{max}^2 + k_g^2\right) - \left(\frac{k_B T}{4\pi\gamma}\right) \ln\left(q_{min}^2 + k_g^2\right). \tag{22}$$

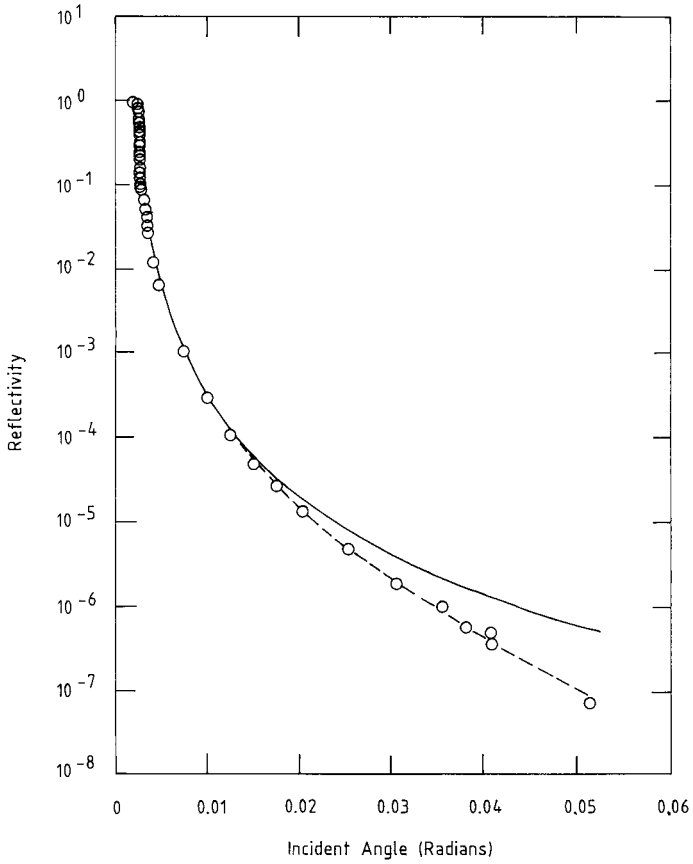

Figure 4. Measured x-ray reflectivity of water as a function of incident angle (o): the solid curve is a calculated curve for a step function density profile, and the dashed curve a fit to the data for a step function density profile and a contribution from CW broadening (reproduced from [47]).

$q_{\min}$ is usually taken as $2\pi/L$, the smallest wavevector that can be sensibly defined (the area of the interface $A = L^2$). This has implications for the experimental arrangement, and will be discussed later in the review. $q_{\max}$ is somewhat arbitrarily defined and is often taken as $q_{\max} = 2\pi/d$, where d is a molecular diameter; this has also been the subject of much discussion. Indeed, the difficulties that arise in extracting σ_0 and $q_{\min}$ will be discussed in the context of some recent data later in the review. $q_{\min}$ and hence $A_{q\,\min}$ are associated with the resolution of the reflectometer. Figure 5 shows a typical arrangement for a horizontal surface reflectometer on a synchrotron radiation source [48].

For liquid surfaces, a monochromatic beam is extracted at an angle to the horizontal plane from the polychromatic synchrotron beam by reflection from a perfect single crystal of Ge or Si (M in figure 5) [48, 62]. An identical analyser crystal directs the reflected beam into the detector, and we assume that the detector slit (S2 in figure 5) defines the resolution. If the spread in angle of the reflected x-rays is less than that angular resolution, then off-specularly scattered photons will be included with the specular reflection. If the resolution is improved, by reducing S2, some of the scattered photons will not be detected and the apparent specular signal will decrease, corresponding to an apparent increase in σ. The dependence upon $q_{\min}$

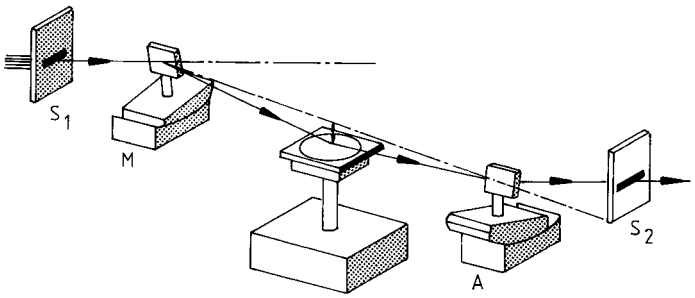

Figure 5. Schematic representation of a horizontal geometry x-ray reflectometer (reproduced from [48]): where *M* and *A* are the single-crystal monochromator and analyser, and S1 and S2 are collimation slits.

is hence of crucial importance, and a detailed evaluation is essential.

If the surface or interface is not perfectly smooth, as is the case with a liquid surface with CWs, then there will be off-specular or diffuse scattering. The decrease in the specular reflectivity appears as diffuse scattering. This provides information about the in-plane correlations of the height fluctuations at the surface, $h(x, y)$. In the distorted-wave Born approximation [63–66], which treats reflection rigorously, the differential scattering cross-section for diffuse scattering is

$$\frac{\mathrm{d}\sigma}{\mathrm{d}\Omega} = r_e^2 A_{xy} |T\ (\theta_0)|^2 |T\ (\theta_1)|^2 \int \rho^2 \langle h\ (x, y)\rangle \exp \mathrm{i} q_{xy} r\ \mathrm{d}x\ \mathrm{d}y \tag{23}$$

where ρ is the average electron density, A_{xy} the area illuminated, $\langle h\ (x, y)\rangle$ the height–height correlation function, and $T(\theta)$ the Fresnel transmission coefficient. Explicit forms of $\frac{\mathrm{d}\sigma}{\mathrm{d}\Omega}$ have been derived for different conditions of surface roughness [63, 64], The diffuse scattering is measured by scanning q_y or by fixing θ_0 and scanning the scattering angle θ_1, and measurements over a wide range of q_y can be achieved, from 10^{-2} to 10^{-5} Å^{-1}. The q_z–q_y plane accessible is shown in figure 6 for a typical experimental arrangement [66], and the principal features are illustrated.

The Yoneda wings that are prevalent close to the region of total reflection [67] are a characteristic feature of a rough surface, and arise from a maximum in the function $|T\ (\theta_0)|^2 |T\ (\theta_1)|^2$ when θ_0 or θ_1 is equal to θ_c. In the context of this review the diffuse scattering is particularly important in identifying and quantifying the contribution from CWs. It provides a powerful complementary measure of thermally excited CWs at liquid surfaces.

For $\theta_0 < \theta_c$ the incident wave is totally reflected, and the incident intensity penetrates the surface as an evanescent wave, which in the absence of absorption decays as $\exp\left(-\frac{z}{\Lambda}\right)$, where $\Lambda \approx \left(\frac{2\pi}{\lambda}\left(\theta_c^2 - \theta_0^2\right)\right)^{-\frac{1}{2}}$, to provide surface scattering from a thin surface layer (typically tens of angstroms). If the surface is a two-dimensional ordered phase, then the evanescent wave will diffract from the in-plane structure when q_{xy} corresponds to an in-plane reciprocal lattice vector (in-plane diffraction). Because of the two-dimensional nature of the ordered phase, Bragg rods of scattering occur (instead of the Bragg spots in normal bulk diffraction) [51, 68]. Daillant *et al* [51] has also exploited this approach to distinguish between the bulk and surface diffuse (or amorphous) scattering in liquid surfaces.

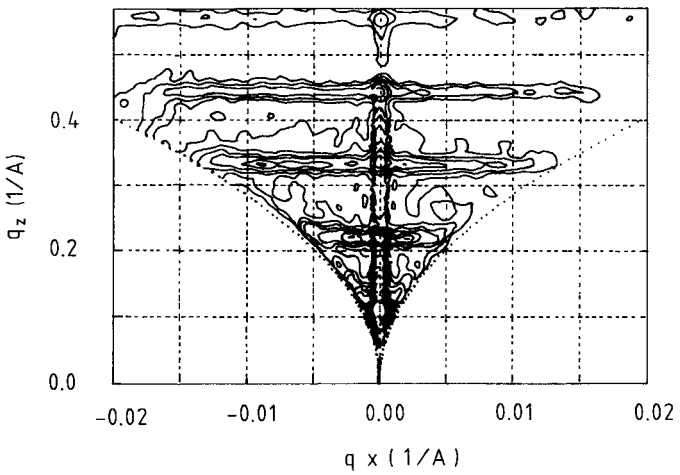

Figure 6. Calculated q_z–q_x map of off-specular scattering for a multi-layer stack, with conformal interfacial roughness (reproduced from [66]).

4. Water and other liquids

Later we shall consider the surface of more complex liquids, which include a range of molecular fluids and liquid metals. However, in this section we discuss results from simpler liquids, predominantly liquid argon, liquid helium, carbon tetrachloride and water. Liquid argon can be thought of as the classical simple liquid, whereas liquid helium is important in that it provides an opportunity to test the theory of quantum fluids. Carbon tetrachloride, although strictly a molecular fluid, has highly symmetrical coordination and so could be expected to have the properties of a simple liquid. Water is, of course, ubiquitous in chemistry and biology, and as a consequence has always attracted considerable attention.

Beaglehole [69, 70] has used ellipsometry to measure the thickness of the surface of liquid argon near its triple point. From the variation of the ellipticity with temperature (in the range 85–120 °C) he was able to make the first comparison of measurement with theory for a simple liquid. The variation of ellipticity, $\bar{\rho}$, with temperature is shown in figure 7.

The solid and dashed curves are calculated curves, where Drude's equation (equation (8)) is modified to include anisotropy in $\varepsilon(z)$ in the interface region, and a form of equation (22) is used to include the intrinsic width of the interface and the CW contribution. The solid curve is calculated for $q_{\max} = \frac{2\pi}{\delta}$ and an experimentally determined surface tension, whereas the dashed curve is for a constant $q_{\max}\left(q_{\min} = \frac{2\pi}{\lambda}\right)$. The analysis produces a thickness δ at 90 K of 7.9 ± 0.5 Å and 15.2 ± 1.0 Å at 120 K, in good agreement with theories that separate the CW contribution from an intrinsic thickness.

Beaglehole [70, 71] used a similar approach to investigate the liquid–vapour interface of carbon tetrachloride, CCl_4, between room temperature and the critical temperature. The motivation for studying carbon tetrachloride was that the highly symmetrical coordination on the molecule meant that it could be treated theoretically as a simple liquid. The data suggest that at large t (where $t = (T_c - T)/T_c$) the surface thickness is determined by CW excitations and by an intrinsic interfacial thickness at small t.

In figure 8 δ/d and L/d are plotted as a function of t, where d is the molecular diameter, δ is a measure of the thickness, and $q_{\max} = 1/L$. At the high and low extremes of t, δ and L vary

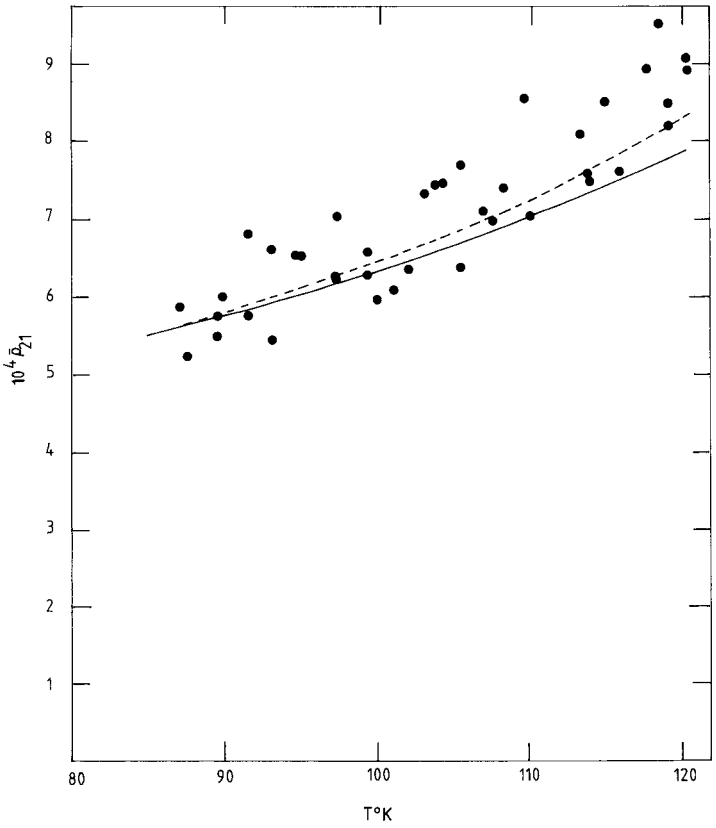

Figure 7. Variation of ellipticity, $\bar{\rho}$, with temperature (●), the full curve represents the predicted variation with $q_{\max} = 2\pi/\delta$ and an experimentally determined surface tension, and the dashed curve a constant $q_{\max}$ (reproduced from [69]).

with approximately the same exponent. The variation in δ/d is from the intrinsic interfacial density profile model [72], whereas the variation in L/d is from the CW model [72]. Both theories have regions of applicability, and some of the implications of this approach have been further discussed by Beysens and Meunier [73]. Braslau *et al* [74] used x-ray reflectivity to extract the intrinsic profile width and the CW contribution (using the CW model), using different instrumental resolutions. The intrinsic width extracted is close to the molecular radius of CCl_4 (3.88 Å), and the spread in values from the measurements with different resolutions is within systematic uncertainties.

Characterization of the structure of the ^{4}He liquid–vapour interface is important for the understanding of the basic features of quantum fluids, and a number of theoretical predictions of the interfacial profile exist [75]. However, due to experimental difficulties, they have remained largely untested. Atomic beam scattering is difficult to interpret due to the complex nature of the interaction, and ellipsometry is sensitive to the width, but not the shape, of the interface. However, Pershan and co-workers [74,76–78] have shown that x-ray reflectivity can be used to probe the shape of the interface. They had to use a specific approach to enhance the sensitivity of the technique. From equation (17), the reflectivity from the bulk air–liquid helium interface scales as ρ_{He}^2 and ρ_{He} is small. Furthermore, to obtain a spatial resolution of < 2 Å a $q_z \sim 0.5$ Å^{-1} is required, and the reflectivity will be $\sim 4 \times 10^{-9}$. To provide that enhanced

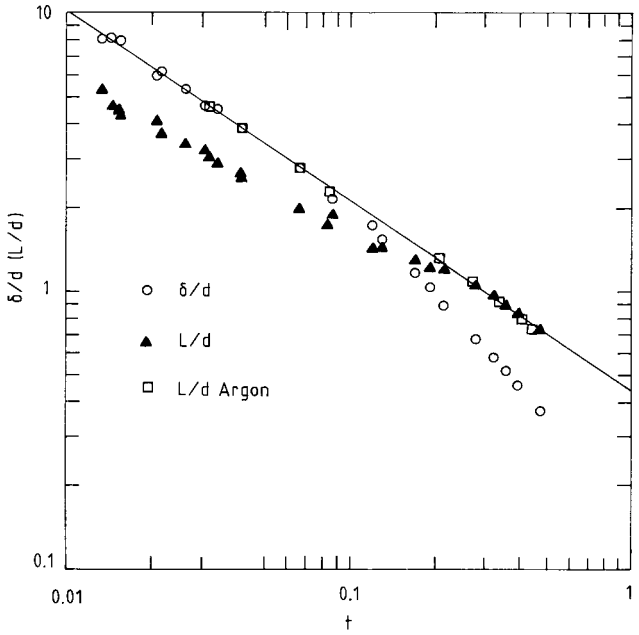

Figure 8. Variation of δ/d and L/d with t, derived from intrinsic and CW models. The straight line is for $\delta_0 = 2.28$ Å and $\nu = 0.683$ (reproduced from [71]).

sensitivity, Pershan *et al* have studied thin helium films on a silicon substrate. They showed that interference between the top and bottom interfaces of the film provided an increase in the signal by a factor ∼20, and that by careful characterization of the silicon surface (by reflectivity, XPS and STM) the extra complexity could be accommodated. Undersaturated films, established as adsorbing films from an unsaturated vapour, provide high-quality films of a range of thickness from 20–200 Å (see figure 9), whereas saturated films support pronounced CW roughness. From a detailed analysis of the profiles the density distribution at the ^{4}He/vapour interface could be extracted with some confidence, and the intrinsic width and CW contributions to the width determined as a function of film thickness (temperature). The helium vapour interface was best described by an asymmetric hyperbolic secant model, in good agreement with the predictions of Stringari and Treiner [75].

The structure of the surface of water has been investigated by x-ray reflectivity [74, 79], diffuse x-ray scattering [51, 82] and ellipsometry [80, 81]. Beaglehole [80] attributed a rapid change in the sign of the coefficient of ellipticity, followed by a slow relaxation back to the equilibrium value with temperature, as due to a surface structural change. However, it arose during non-equilibrium conditions and was not present when dissolved gases were removed, and has not, to the author's knowledge, been pursued further. In their pioneering work Braslau *et al* [79] measured the roughness of the liquid–vapour interface of pure water by x-ray reflectivity. With measurements down to a reflectivity $\sim 7 \times 10^{-8}$ they obtained a rms roughness of 3.2 Å, interpreted from the CW model and in agreement with their estimated value which took into account the upper and lower cut-offs, $q_{\min}$, $q_{\max}$. Subsequently, with additional data and a more detailed analysis [74] (using the CW model), they obtained an estimate of the intrinsic profile width (1.8 Å) and the CW contribution, with the intrinsic width close to the molecular diameter (1.93 Å). Townsend and Rice [83] obtained a width

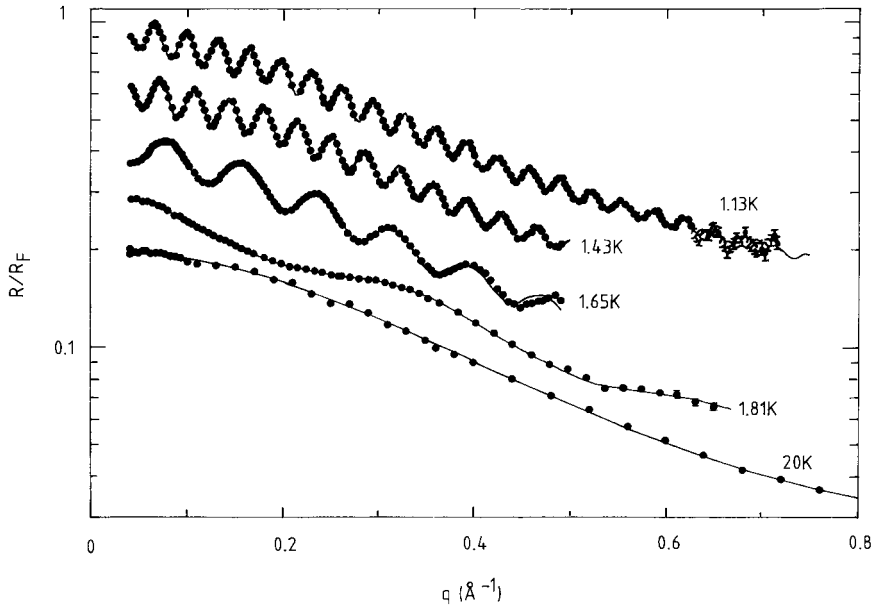

Figure 9. $R(q)/R_F(q)$ for undersaturated He^4 films on silicon. The curves are fits to the data for an asech model convoluted with CWs, for film thicknesses of 192 Å ($T = 1.13$ K), 175 Å ($T = 1.45$ K), 80 Å ($T = 1.65$ K), 18 Å ($T = 1.81$ K), and at $T = 20$ K without an adsorbed film (reproduced from [77]).

of the interfacial density profile of water of 3.45 Å from molecular dynamics calculations. It was found that the molecules in the outermost region of the liquid–vapour interface tend to lie with the molecular dipole in the plane of the interface. Furthermore, as the density drops in the transition region the tetrahedral structure breaks up into dimerization. Such detail in beyond current experimental techniques. More recently, Schwartz *et al* [82] have combined both x-ray reflectivity and diffuse scattering to obtain a more complete understanding of the surface of water. Specular reflectivity measurements at three different resolutions gave simultaneous fits with an intrinsic width of zero and with one value of $q_{max}(\pi/1.4)$. In addition, the diffuse scattering measurements (see figure 10) agreed with the theoretical form for CWs, with no significant adjustable parameters. Both measurements show that CWs contribute to the width of the water–vapour interface with wavelengths from 400 to 80 000 Å, as expected from theory (equation (22)). This represents the most complete study using scattering techniques, and demonstrates the importance of a correct interpretation of q_{min}, and q_{max}. This is accomplished by making measurements at different instrument resolutions, and by the complementary interpretation of the diffuse scattering. Daillant [51] has made more extended diffuse scattering measurements on the water–vapour interface, separating out both the q_x and q_y contributions, and shown that they are well described by CWs.

5. Surface melting and crystallization

Both x-ray and light scattering have been extensively used to study crystallization, growth and wetting phenomena at surfaces in a variety of systems [84]. In particular, melting and pre-melting transitions in binary mixtures, and the consequences of approaching critical points, has been a vast area of activity [7], and is beyond the scope of this review. An exception to

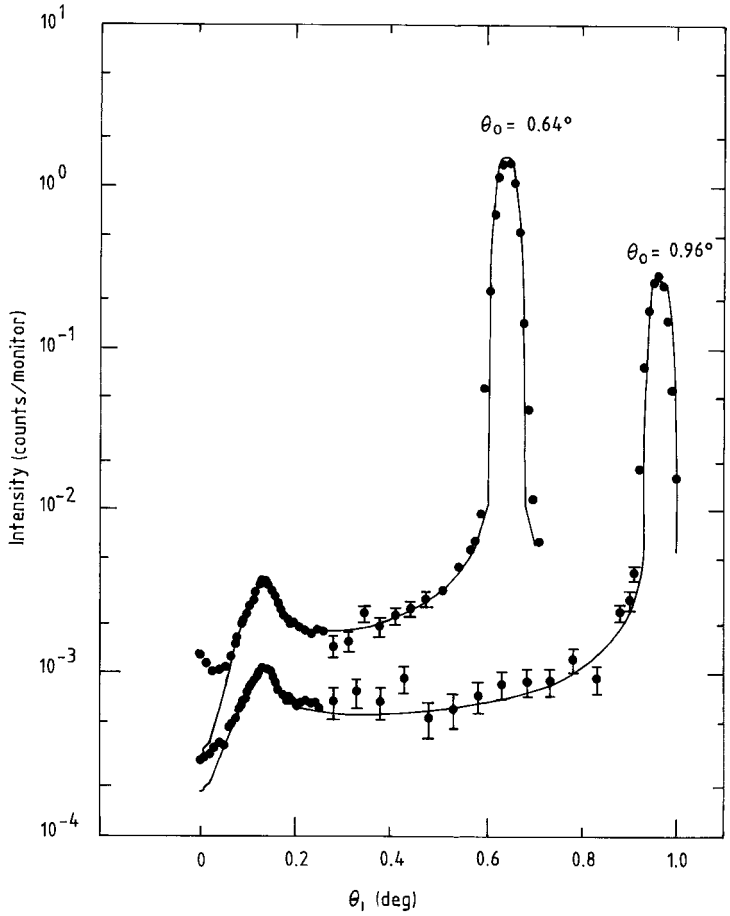

Figure 10. Scattered intensity, in the plane of incidence, as a function of detector angle θ_1, for an incident angle $\theta_0 = 0.64^\circ$ and 0.96° for water. The solid curves are calculated curves as discussed in the text (reproduced from [82]).

this is the consequence of pre-melting and surface crystallization, which is discussed in the context of simple liquids and molecular fluids. In many physical systems, surface melting, where the surface solidifies at temperatures lower than the bulk, is usually observed. This is due to the reduced degree of confinement, and hence increased entropy of the molecules at the surface compared with the bulk. However, in some specific systems, liquid crystals, alkanes and alcohols, the opposite is observed. That is, they exhibit surface freezing; the surface orders at a temperature above the bulk ordering temperature. This is discussed in more detail in the context of the surface of alkanes and alcohols in the next section.

Pre-melting or surface melting of the ice–solid or ice–water (vapour) interfaces has attracted much interest and provided a formidable experimental challenge, and recent developments in this area are discussed here. Using ellipsometry and optical reflectivity Beaglehole and Wilson [85, 86] and Elbaum *et al* [87] have produced definitive experimental evidence for pre-melting and surface melting. Beaglehole and Wilson [85, 86] used ellipsometry to investigate pre-melting at the ice–glass interface. The coefficient of ellipticity, $\bar{\rho}$, was used as a sensitive measure of the interfacial profile and width. Extreme care in

the experimental design was required to eliminate other contributions to $\bar{\rho}$, such as surface roughness, and imperfections in the crystal and in the containment vessel. Slow controlled crystal growth and sensitive temperature control were required. The interface between ice and smooth clean glass showed no evidence of pre-melting, whereas pre-melting was observed at interfaces with roughened glass surfaces. Contamination, contrived by the addition of NaCl, also showed pre-melting with increasing surface concentration of electrolyte. A rough, but hydrophobic, surface showed no evidence of surface pre-melting. The growth of the interfacial water layer with ΔT was followed for both roughened surfaces and impurity, and showed different growth laws.

Elbaum *et al* [87] used optical reflectivity to measure the thickness of water films on the surfaces of isolated ice crystals at temperatures below 0 °C. Different crystal facets were investigated. On prismatic facets no pre-wetting was observed, and as the triple point is approached water drops are formed. On the basal facet incomplete surface melting occurs, and a film thickness ∼200 Å was found. The addition of air caused the film thickness to diverge, and caused complete surface melting.

6. Molecular fluids (alkanes and alcohols)

The nature of the liquid–vapour interface of molecular fluids has additional complexity associated with molecular orientation in addition to the interfacial density profile. Although much of the theoretical effort has been aimed at predicting orientational order in relatively small diatomic molecules [21–27], and in water [28, 29], a perhaps unexpected manifestation of changes in molecular orientation at the interface is the observation of surface freezing or crystallization in alkanes and alcohols [88–95]. This is opposite to the normal expectation of surface melting or pre-melting as discussed in the previous section, and has been found to occur in liquid crystals, alkanes and alcohols. It has been observed by x-ray reflectivity, grazing incidence diffraction [91–97], ellipsometry [90], surface tension [88], and other macroscopic phenomena [89], such as the stabilization of foams. The study of surface freezing has developed into a rich area of interest, and a number of recent detailed studies are discussed later in this section.

X-ray reflectivity and 'off-specular scattering' measurements have been made on a range of alcohols and alkanes, to extend the comparison with CW theory to fluids comprised of larger molecules [96, 97]. Sanyal *et al* [96] used x-ray specular reflectivity and 'off-specular' scattering to investigate the liquid–vapour interface of ethanol at room temperature. They obtained quantitative agreement for both the specular and 'off-specular' data with the predictions based on the standard continuum theory for CWs [72]. As a result of the reduced dimensionality, the density–density correlations induced by the CW fluctuations are expected to show a power law dependence on q, and this has been demonstrated in figure 11.

The peak in the wing of the diffuse scattering, for $q_z = 0.1$, arises from Yoneda scattering (as discussed earlier), and the fitted curves are calculated using explicitly (from equation (23))

$$I = I_0 \frac{q_c^4}{16} \frac{1}{q_z^2} \left[\frac{1}{2k_0 \sin\alpha} \right] \exp\left[-q_z^2 \sigma_{\text{eff}}^2\right] \frac{1}{\sqrt{\pi}} \Gamma\left(\frac{1-\eta}{2}\right) |F| \times \left(\frac{1-\eta}{2}; \frac{1}{2}; \frac{q_y^2 L^2}{4\pi^2} \right) |T(\theta_0)|^2 |T(\theta_1)|^2 \tag{24}$$

where I_0 is the incident beam intensity, k_0 the incident wavevector, q_c the critical wavevector, $\Gamma(x)$ the gamma function, $|F(x; y; z)|$ the Kummer function, $\eta = \frac{1}{2} B q_z^2$, $B = \frac{k_B T}{\pi\gamma}$, γ is the

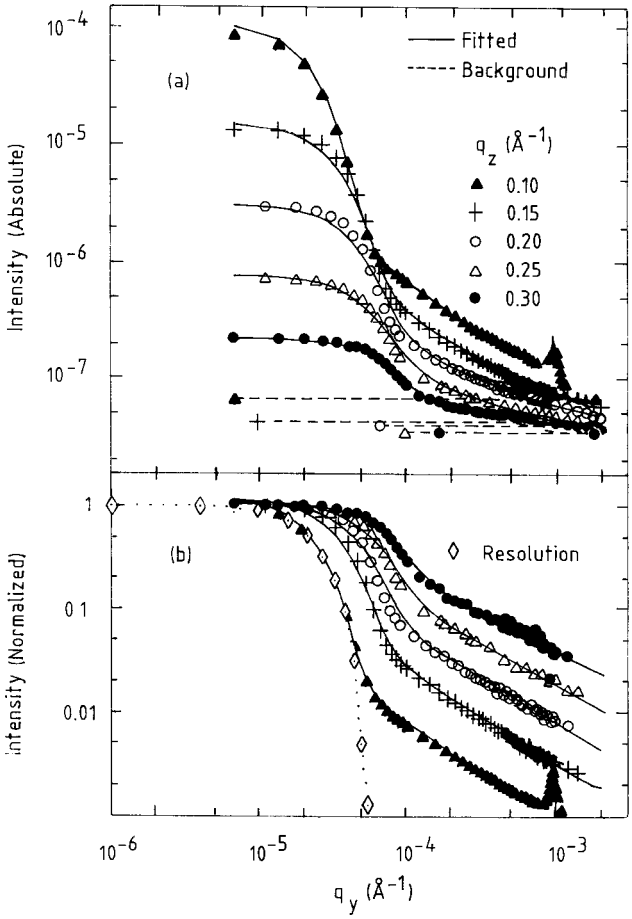

Figure 11. Absolute scattered intensity versus q_y (for different values of q_z) for ethanol at room temperature. The solid curves are calculations, as described in the text (reproduced from [96]).

surface tension and, for $\kappa \ll q_{\min}$,

$$\sigma_{\text{eff}}^2 = \frac{1}{2} B \ln \left[\frac{e^{\gamma_e}}{2\pi} q_{\min} L \right]. \tag{25}$$

γ_e is the decay of the surface density–density correlation function, and $q_{\min}$ the upper wavevector cut-off for the CWs. The analysis of the specular reflectivity and off-specular scattering gave a σ_{eff} of 6.9 ± 0.2 Å and an upper wavevector cut-off of $\sim \pi/d$ (where d is the molecular diameter of 5.7 Å for ethanol), with no other adjustable parameters.

The original continuum theory model [72] has been modified to include an intrinsic profile of finite width in the form of equation (22). If the gravitational term k_g is small then it reduces to the form used by Ocko *et al* [97],

$$\sigma^2 = \sigma_0^2 + \sigma_{\text{cw}}^2 = \sigma_0^2 + \frac{k_0 T}{2\pi\gamma} \ln \left(\frac{q_{\min}}{q_{\max}} \right). \tag{26}$$

$q_{\min}$ is determined by the instrumental resolution (the longest coherence length resolvable) and $q_{\max} \sim \pi/d$ (where d is the molecular size). The resolution dependence of the second term in

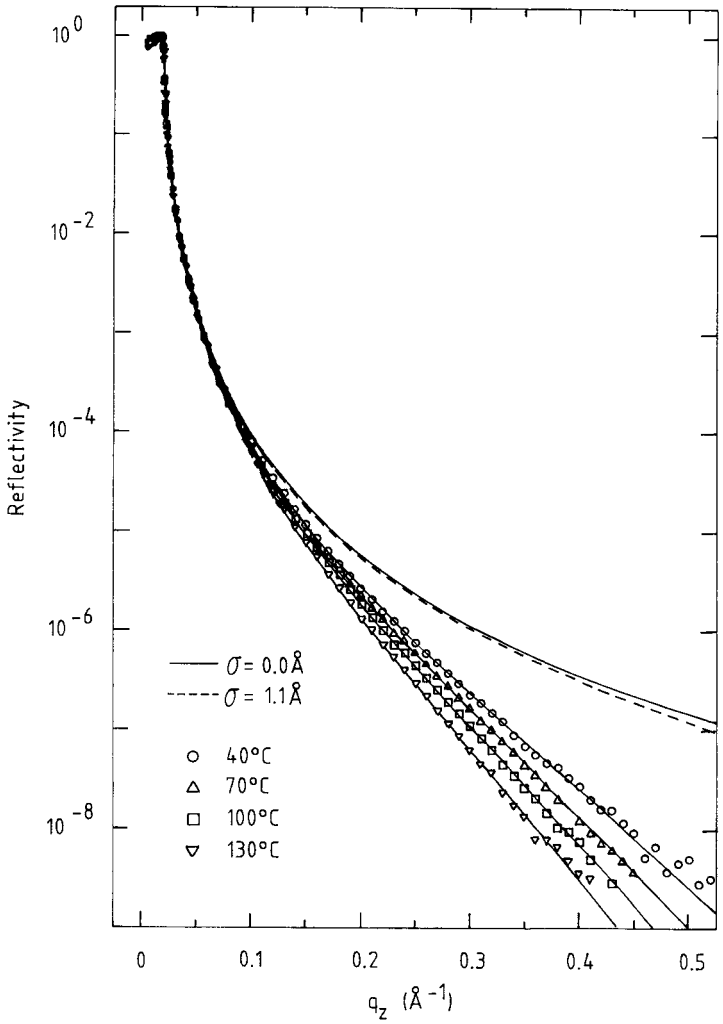

Figure 12. X-ray reflectivity of C_{20} at $T = 40, 70, 100$, and 130 °C. The curves through the symbols are fits as discussed in the text. The solid and dashed curves represent the Fresnel reflectivity for a sharp step function and an interfacial width, σ_0, of 1.1 Å (reproduced from [97]).

equation (26) has been verified by Braslau *et al* [74] for water and CCl_4, and a number of studies have shown the applicability of the CW model on liquids of similar molecular size [51,79,96]. However, the magnitude and origins of q_{max} and σ_0 have not been fully understood. To address this Ocko *et al* [97] have measured the x-ray reflectivity from a range of different chain length alkanes (from C_{20} to C_{36}) over a wide temperature range (see figure 12 for the data for C_{20} in the temperature range 40–130 °C).

The data are all consistent with the hybrid CW model described by equation (26), with q_{max} and σ_0 as variables. q_{max} and σ_0 are strongly coupled in the fitting procedure, but a shallow minimum in χ^2 provided a unique combination; and q_{max} and σ_0 are found to be independent of temperature. C_{20} gave a $\sigma_0 \sim 1.5$ Å and a $\pi/q_{max} \sim 7.1$ Å (considerably larger than for water (1.9 Å), ethanol (2.5 Å), and CCl_4 (3.4 Å)). For C_{36} a $\sigma_0 \sim 1.1$ and a $\pi/q_{max} \sim 11.6$.

The ratio of π/q_{max} for C_{20} and C_{36} is comparable with the ratio of chain lengths. The hybrid model, which accounts for additional roughness due to the finite molecular size, is in good agreement with the data, and the Buff *et al* [72] model is found not to be adequate.

Meunier [38] has used optical reflectivity and ellipsometry to investigate the effect of thermal fluctuations on the structure of the liquid–vapour interface. Measured and calculated ellipticities for a range of fluids, including water, CCl_4, and different alkanes and alcohols, were in modest agreement. The ellipticities were calculated by mode coupling theory. Ocko *et al* [97] discussed the applicability of mode coupling in relationship to their data. They concluded that the influence of mode coupling was small, and that it effectively reduces to an expression similar to that for the hybrid model (equation (26)) with the exception that q_{max} does not explicitly depend on molecular size $\left(q^{mc}_{max} = \sqrt{\frac{8\pi\gamma}{3k_BT}}\right)$.

Earnshaw and McGiven [42,43] used quasi-elastic light scattering to study the surface of water and ethanol: from the observed wavenumber dependence of the frequency and damping constants of the CWs, they extracted values for surface tension and viscosity. The results were in good agreement with both theory and literature values.

Surface freezing or crystallization, that is surface ordering at a temperature above the bulk ordering temperature, is an unusual phenomenon which is seen in liquid crystals, and more recently in a range of alkanes and alcohols. Whereas x-ray reflectivity and grazing incidence diffraction measurements have revealed a solid monolayer of molecules, surface tension [88] and other macroscopic phenomena [89] have also shown the existence of surface freezing in liquid alkanes. Wu *et al* [88], from a discontinuity in the temperature dependence of the surface tension (figure 13), have revealed the surface freezing in liquid alkanes.

The discontinuity is attributed to the formation of a solid monolayer of molecules at up to 3 °C above the bulk freezing point. The surface tension, γ, is the excess free energy of the surface over the bulk, such that

$$\frac{d\gamma}{dT} = -(S_s - S_B) \tag{27}$$

where S_s, S_B are the surface and bulk entropies. The negative slope for $T > T_s$ (T_s is the surface freezing temperature) arises because the surface is liquid and $S_s > S_B$, and for $T < T_s$ the surface ordering reduces S_s such that $S_s < S_B$ and the slope is positive. The surface phase is found to exist for carbon numbers $14 < n < 50$. The authors attribute the lack of surface phase for $n < 14$ to surface melting behaviour. They have developed a simple thermodynamic model, based on bulk latent heats and consideration of surface energy, which predicts well the dependence on n of the surface tension and ΔT (where $\Delta T = T_s - T_f$, T_f is the bulk freezing temperature) (see figure 14).

For $T < T_s$

$$T_f = \gamma'_\infty + \frac{\beta}{n^2} \tag{28}$$

where γ'_∞, β are constants, and the expression is derived by assuming an excess energy (from van der Waals interactions proportional to the inter-layer distance and hence n) as the surface monolayer has no overlayer interaction like the bulk. For $T > T_s$ the liquid surface has a relationship of the form,

$$\gamma_T = \gamma_\infty - \frac{\alpha}{n^{\frac{2}{3}}} \tag{29}$$

from free-volume considerations. Both expressions agree well with the data in figure 14.

Gang *et al* [89] have reported two macroscopic manifestations of surface crystallization. The formation of a foam in a liquid alkane (in the absence of surfactant) is attributed to a

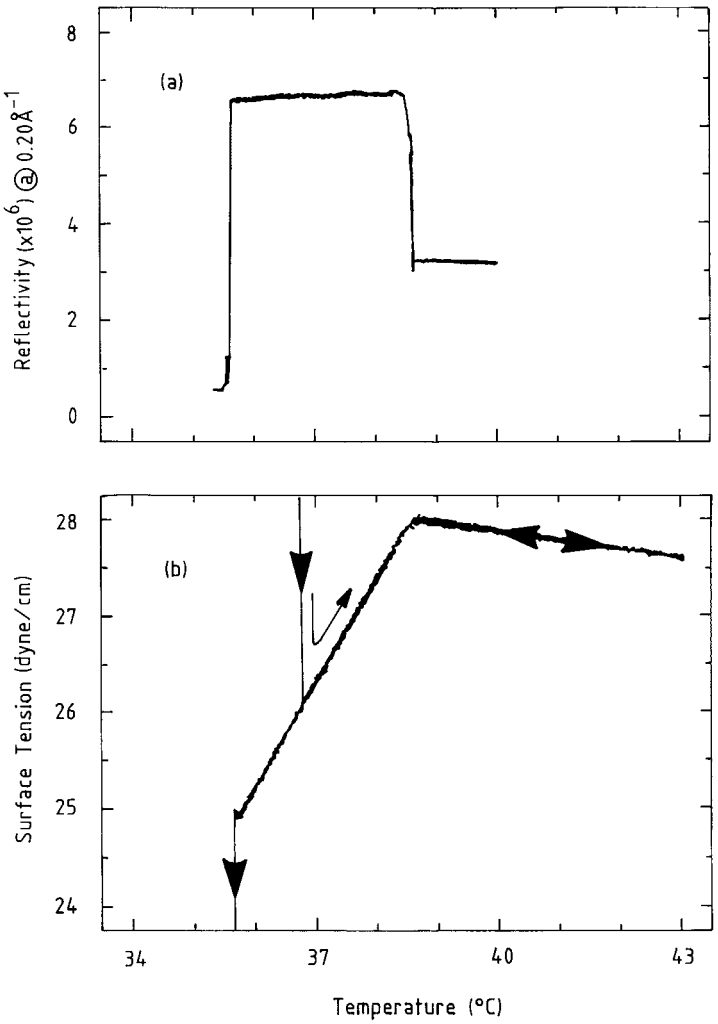

Figure 13. Temperature scan for C_{20} of (*a*) x-ray reflectivity at $q_z = 0.2$ Å^{-1}, and (*b*) surface tension (showing heating and cooling cycles) (reproduced from [88]).

stabilization of the foam due to the presence of a surface crystalline phase. Rapid lateral movement of dust particles on a liquid alkane surface as it cools is due to the onset of surface crystallization. Surface crystallization causes a surface tension gradient, which induces surface flow (Marangoni effect).

Pfohl *et al* [90] investigated surface freezing at the alkane/air interface by ellipsometry and surface tension. A small change in the ellipticity was attributed to the transition from an isotropic liquid surface to a well ordered monolayer. They discuss the surface freezing as a transition from nematic-like to smectic-like ordering. However, this is not borne out by the overwhelming evidence from x-ray reflectivity and grazing incidence diffraction.

Sinha *et al* [91–97] have made a detailed study, using surface tension and x-ray reflectivity and grazing incidence diffraction, of the surface freezing in a wide range of alkanes and alcohols. The simplest and most direct observation of the surface ordered phase is in the x-ray

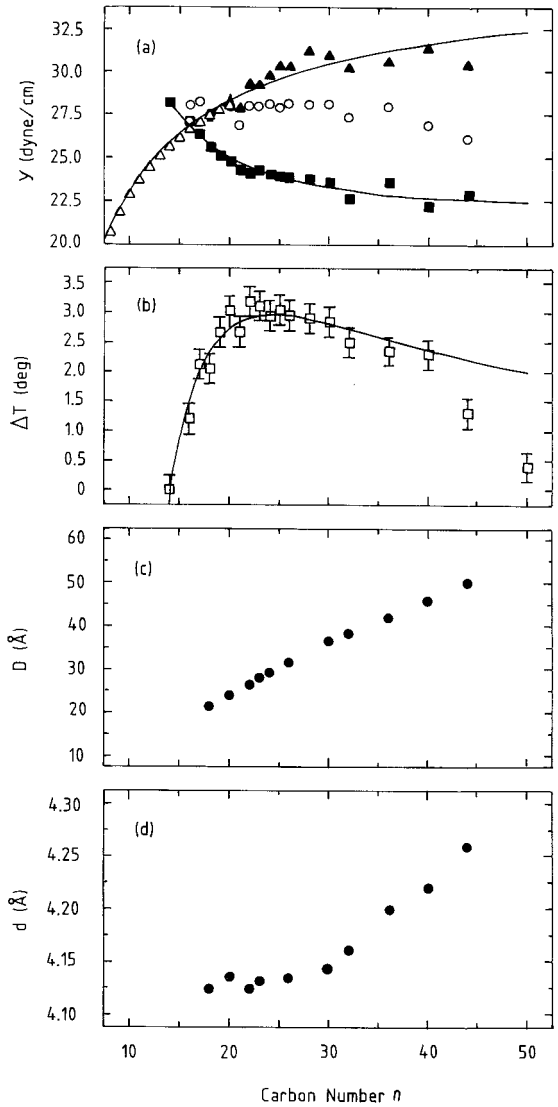

Figure 14. Variation with chain length (n) for (a) surface tension, γ, measured at T_F (□), T_S (o), and $T = 30\,^{\circ}\mathrm{C}$ (△). Curves are theoretical curves as described in the text, (b) ΔT, (c) surface monolayer thickness (from reflectivity), and (d) grazing incidence measured lattice spacing of hexagonally ordered surface layer (reproduced from [92]).

reflectivity data (see figure 15).

Figure 15 shows the reflectivity data for C_{18}, C_{20} and C_{24} [91], and similar data were measured for alkanes up to a chain length of 44 [93]. For $T > T_s$ the reflectivity is described by CW theory, with a width σ described by equation (26), consistent with measurements of other liquids comprised of smaller molecules. σ was ∼4.4 Å and the CW contribution for two different liquids [1, 2] scaled as the ratio of the surface tensions,

$$\frac{\sigma_{cw,1}}{\sigma_{cw,2}} = \sqrt{\frac{\gamma_2}{\gamma_1}}. \tag{30}$$

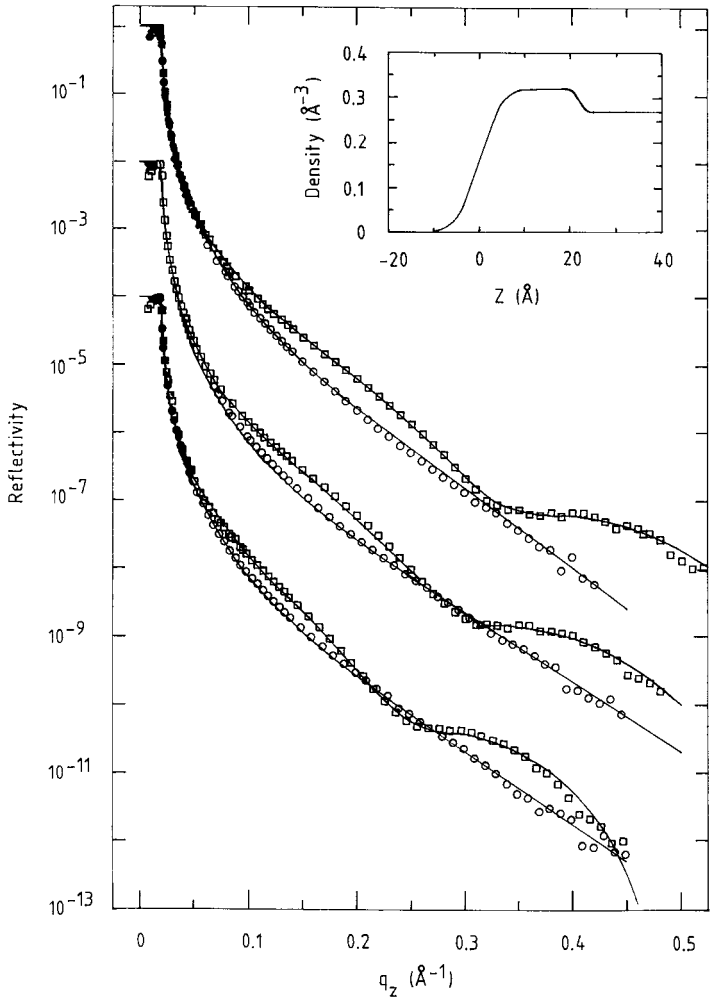

Figure 15. X-ray reflectivities for C_{18}, C_{20}, and C_{24}, for (o) liquid surface phase, and (□) surface monolayer. The solid curves are fitted curves, for models as described in the text. For the surface monolayer the model electron density profile is shown in the inset (reproduced from [91]).

In the surface ordered phase pronounced fringes are formed, consistent with the formation of a single layer of thickness t. The thickness was close to the fully extended chain length, but consistent with a tilt angle which was dependent on the chain length of the alkane. The dependence of the chain length was found to be different for $n > 30$ and $n < 30$, consistent with different surface ordering. The density of the surface layer was found to be ∼20% higher than that of the bulk liquid alkane, and comparable to that for a bulk ordered rotator phase. The quality of the data was such that the reduced electron density of the terminal CH_3 was included in the modelling, and provided noticeably improved fits. Monitoring the x-ray reflectivity (at a fixed q_z value) as a function of ΔT (see figure 13) provided a direct measure and quantification of both T_s and T_f. The abrupt formation of the denser surface monolayer at T_s is seen in the increase in reflectivity. The reduction in the reflectivity at T_f is associated with a dramatic increase in surface roughness when the bulk liquid freezes. More detailed, complementary,

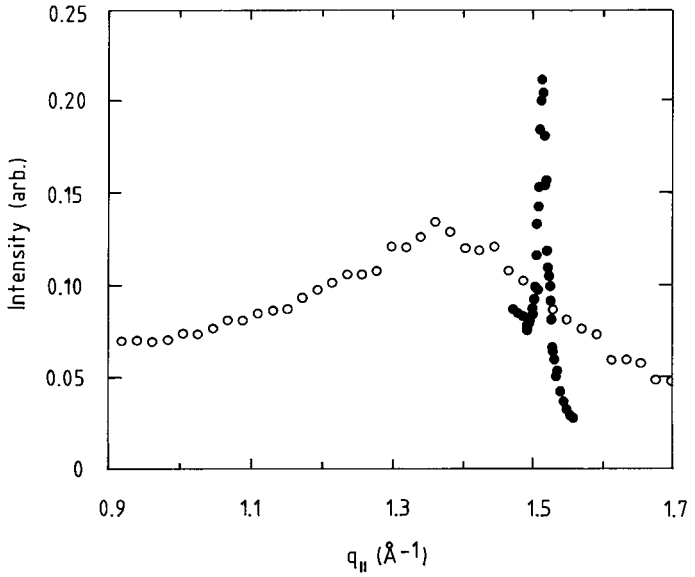

Figure 16. In-plane x-ray diffraction from C_{20} alkane liquid, (o) at high temperature, showing the bulk liquid peak, (●) surface crystalline monolayer, showing a resolution-limited Bragg peak (reproduced from [91]).

and consistent information about the in-plane order is obtained from the grazing incidence diffraction measurements (see figure 16).

For $T > T_s$ the broad peak at $q_{\parallel} = 1.35$ Å^{-1} is typical of liquid alkanes. When the ordered monolayer appears at T_s a sharp Bragg peak appears at $q_{\parallel} = 1.513$ Å^{-1}, with a width that is indicative of a large domain size. From a detailed analysis of the diffraction data it was concluded that different ordered phases exist, depending upon the chain length of the alkane. For $n < 30$ the ordered layer is hexagonally packed with vertically aligned molecules. For $30 < n < 44$ the molecules are tilted towards nearest neighbours, towards next-nearest neighbours for $n > 44$, and the tilt angle varies with n. For $n < 44$ the surface layer is a rotator phase, and for $n > 44$ a non-rotator crystalline phase. The single ordered monolayer formed at T_s persists down to T_f, and is hence considered as a partial wetting layer. The disappearance of the surface phase for $n < 14$ is attributed to a surface freezing to surface melting transition. The decrease in ΔT for larger n and the eventual disappearance of the surface phase for $n > 44$ is attributed to the frustration caused by the greater likelihood of gauche chain conformations. Although characterized in some detail, a quantitative microscopic theory for the monolayer formation and its n and T dependence is not yet available. In particular, why surface freezing is favoured over surface melting is not fully understood. It has been postulated that the lower density of the terminal CH_3 group imparts surface activity, and that subsequently surface enrichment induces preferred order or alignment at the interface.

Sinha *et al* [94, 95] have extended the x-ray reflectivity and grazing incidence diffraction measurements to other systems, notably to a range of different chain length alcohols, in order to shed further light on the surface freezing mechanism. They observed the same surface freezing in both dry and hydrated alcohols by x-ray scattering and surface tensiometry, but with some important differences. As observed with the alkanes, the formation of the surface ordered layer is indicated by abrupt changes in surface tension and x-ray reflectivity. The x-ray

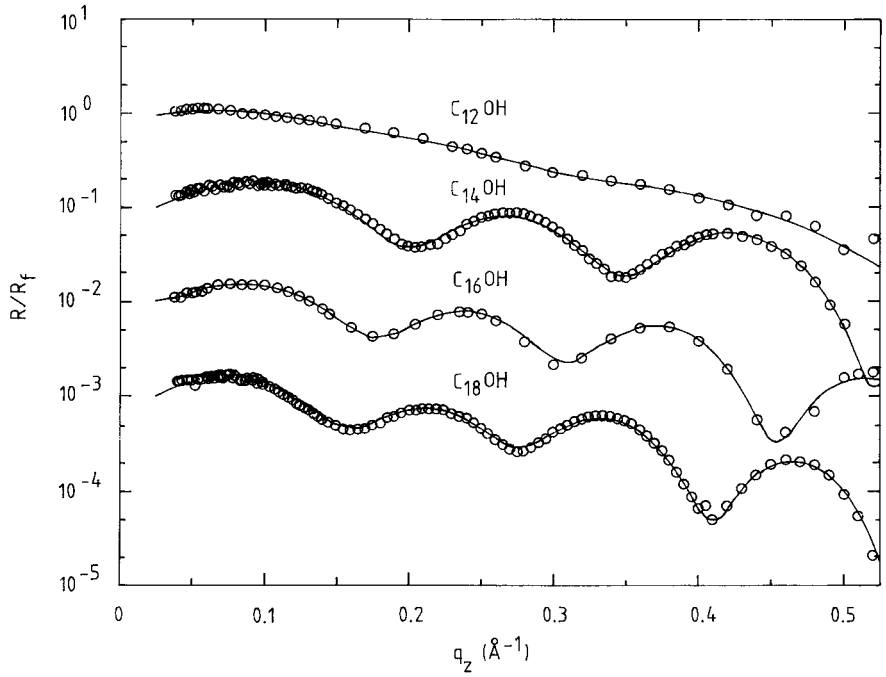

Figure 17. X-ray reflectivity (normalized to the Fresnel reflectivity) for hydrated alcohols ($C_{12}OH$ to $C_{18}OH$). The curves are fits to the model described in the text (reproduced from [95]).

reflectivity data showed well defined interference fringes, consistent with a layer of increased density, and thicker than the equivalent alkane layer by a factor of two. The layer thicknesses (for $n = 20$, 24 and 28, t is ∼51, 61 and 70 Å) indicate that a bilayer is formed. Hydration is found to have an impact on the surface ordering. It swells the bilayer by ∼2.5 Å, due to water being incorporated into the headgroup region. It also increases the transition temperature, T_s, and the temperature and chain length ranges over which surface crystallization is observed (see figure 17).

Figure 17 shows the normalized reflectivity (normalized to the Fresnel reflectivity) for several hydrated alcohols. When dry $C_{12}OH$ and $C_{14}OH$ show no surface ordered phase, but do when hydrated; and for $C_{16}OH$ ΔT increases from 0.15 to 2.0 °C when hydrated. Grazing incidence diffraction again shows that the ordering in the plane is hexagonal, with nearest-neighbour tilting for $n < 24$ and next-nearest-neighbour tilting for $n > 24$. Hydration also has an impact on the in-plane order observed in the surface phase (see figure 18).

For $n = 18$, and 22 the packing remains hexagonal and the molecules untilted, and hydration results in a small (∼2%) in-plane lattice expansion. At $n = 28$, the Bragg rod measurements (a scan in q_z for a fixed value of $q_\parallel$) suggest that hydration induces a transition from a crystalline to a rotator surface phase. The consequence of hydration is to stabilize the surface layer. This was shown to result from differences in hydration between the bulk and surface in their liquid phase, and a modified Gibbs adsorption rule was devised to account for this.

In addition to the differences between the alcohols and alkanes, and the role of hydration, there are some differences in the chain length dependence. For the dry alcohols the surface freezing is only observed for even carbon numbers. This is in contrast to the alkanes, where no

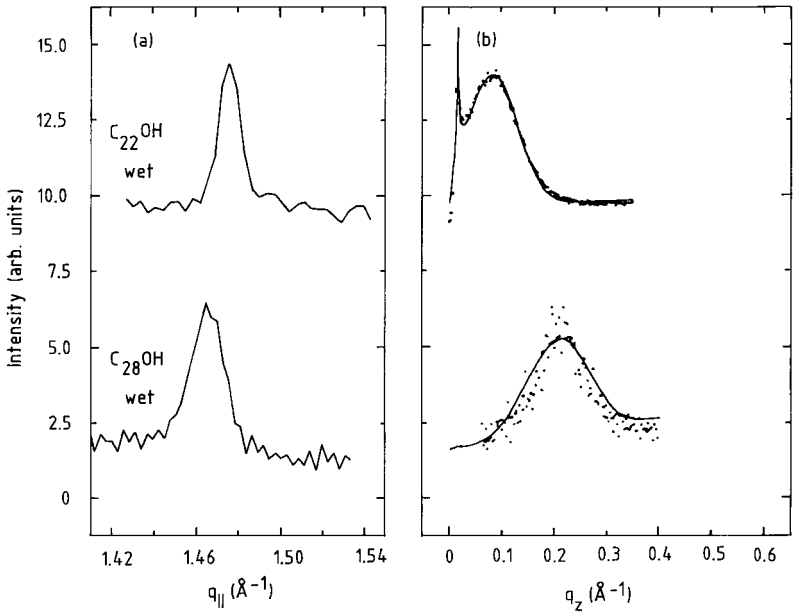

Figure 18. In-plane x-ray diffraction from hydrated alcohols, $C_{12}OH$ and $C_{28}OH$ (reproduced from [95]).

odd–even effects are observed. Odd–even effects also do not occur in the bulk for the alcohols, and the reason for the odd–even effect in surface freezing was attributed to differences in the orientation of the terminal OH relative to the molecular axis.

7. Liquid metals

Progress in understanding the structure of liquid metal surfaces has been hampered by a lack of suitable experimental techniques. Only recently has x-ray reflectivity on third-generation synchrotron x-ray sources been able to access the q region relevant to the predictions of surface layering on an atomic scale. The pioneering work of Chu and Rice [98] provided some direct information, but was limited only to an estimate of the surface 'thickness'. There have also been several other experiments reported, providing interesting but indirect information about surface structure, such as surface tension [99]. Hence, until the recent x-ray reflectivity studies [100–109], our understanding of liquid metal surfaces was relatively primitive. The well known screened pseudo-atom model [13], which represents the potential energy of the metal as a sum of effective pair-wise inter-ionic potentials plus a volume dependent 'self-energy' contribution, provides a good description of bulk properties of many metals, but appears to be inadequate for describing the interface. The Jellium model [31] has provided a good starting point and much progress has been made theoretically [30, 31] and with computer simulations [32–34]. The two-component nature of the fluid, the strong Coulombic interactions and pronounced density variation at the interface were predicted by theory [30, 31] and computer simulation [32–34] to give rise to atomic layering at the surface. The relatively subtle variation of the fluctuations and correlation length of the surface ordering ($<$10 Å), are responsible for the experimental challenge. However, in recent years Pershan and co-workers [100–109] have performed a series of pioneering experiments on liquid gallium and

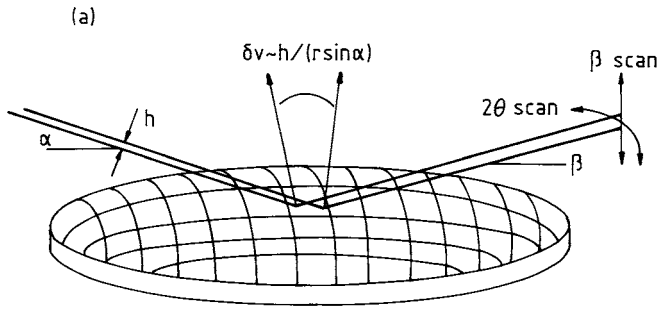

Figure 19. Schematic diagram of a curved liquid surface, illustrating scan directions for reliable extraction of specular reflectivity. The x-ray footprint on the liquid surface strikes the surface where the local normal is at an angle u to the vertical, with a local radius v, β scans (in the plane of reflection), and 2θ scans (normal to the plane of reflection) are used to profile the reflection.

mercury, and established unambiguously the existence of surface-induced atomic layering in liquid metals.

Surface-induced atomic layering would give rise to an interference maximum in the specular reflectivity of x-rays at high q_z. If the ordering is of a similar length scale to that giving rise to the first peak in the bulk liquid metal structure factor, then it is necessary to measure to a q_z value of >2.0 Å^{-1}. This is in itself a formidable challenge, but other technical difficulties also have to be overcome.

In their first reported study, Kawamoto *et al* [100] measured the x-ray reflectivity from the surface of liquid gallium out to a $q_z \sim 0.5$ Å^{-1}. The small deviation from the theoretical Fresnel reflectivity for an ideally sharp interface was consistent with an interfacial width for the electron density profile of <1.3 Å, and the reflectivity was not measured to sufficiently high q_z to observe surface layering. They were, however, able to overcome or circumvent a number of the experimental difficulties. The measurements were made in a UHV chamber (partial O_2 pressure $<10^{-11}$ Torr) and surface oxide was removed with a mechanical scraper and argon ion sputtering. Suppression of mechanically excited surface waves (a particular problem due to the high surface tension) was overcome by using a shallow sample (<0.3 mm), but the high surface tension and the need to use a small sample area gave rise to a curved sample surface. This was accommodated by devising a combination of angular and height scans which has enabled the specular reflectivity to be properly extracted (see figure 19).

Subsequently, using the same approach Regan *et al* [101] were able to measure the specular reflectivity from a liquid gallium surface to a $q_z \sim 3.0$ Å^{-1} (see figure 20).

At the high Q_z values achieved by Regan *et al* bulk diffuse scattering is a major contribution to the measured reflectivity, and is subtracted by performing 'off-specular' scans at each q_z value [105]. The importance of the *in situ* cleaning of the surface is illustrated in figure 21. The previous data [100] measured to much lower q_z values are also shown. The data show no appreciable deviation from Fresnel's law until a $q_z > 2.0$ Å^{-1}, where a pronounced maximum is observed. This is shown very clearly when scaled by the Fresnel reflectivity. The data at high q_z were analysed using the kinematic approximation (equation (17)) with $\frac{\langle\rho(z)\rangle}{\rho_\infty}$ as an exponentially decaying sine wave and an error function interfacial profile, such that

$$\frac{\langle\rho\,(z)\rangle}{\rho_\infty} = \operatorname{erf}\left[\frac{(z-z_0)}{\sigma}\right] + \theta\,(z)\,A\sin\left(\frac{2\pi z}{d}\right)\mathrm{e}^{-z/\zeta} \tag{31}$$

where σ is the interfacial width, $\theta(z)$ is a step function, A the amplitude and d the period of the sine wave, and ζ the decay correlation length (see inset in figure 20). The fit to the data gave

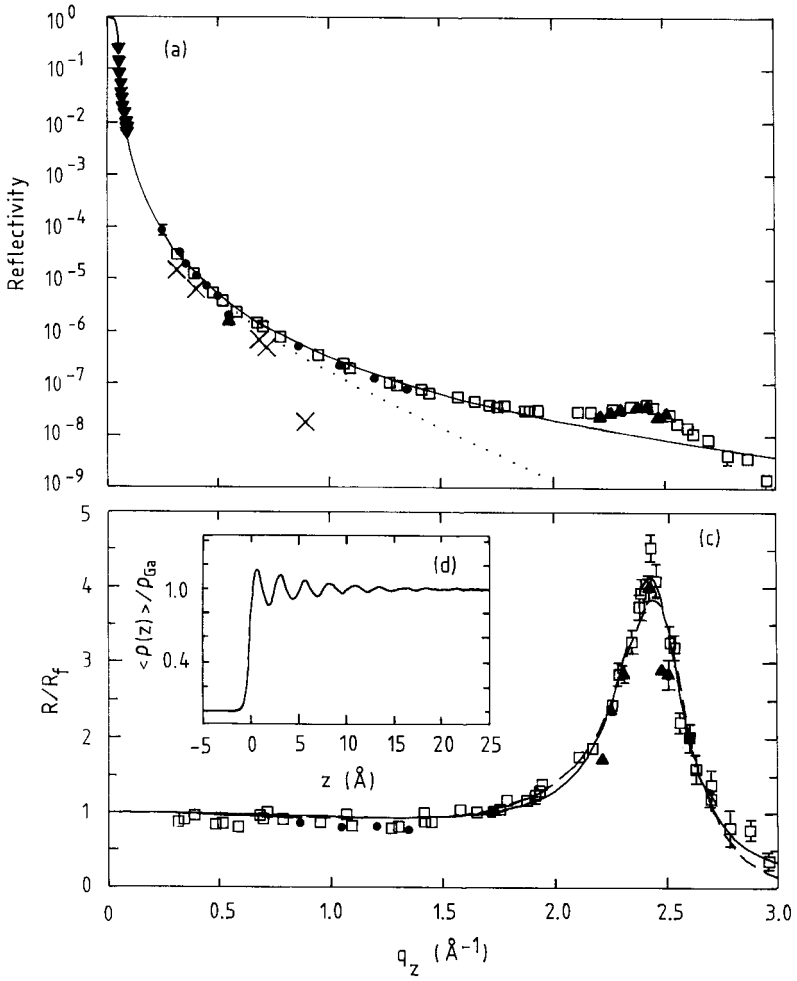

Figure 20. (*a*) Measured x-ray reflectivity for liquid gallium, (*x*) data measured prior to surface cleaning, solid curve is the Fresnel reflectivity; (*b*) reflectivity normalized to the Fresnel reflectivity, solid curve is a calculated curve for the electron density distribution shown in (*c*) and described in the text (reproduced from [101]).

an interlayer spacing $d \sim 2.56$ Å and a decay length ∼5.8 Å (corresponding to ∼2 atomic diameters). A more sophisticated model, based on the distorted crystal model, used also for liquid mercury (see later in this section), produced similar results. The interlayer spacing is less than the mean neighbour spacing in the bulk liquid, as expected from the stacking of neighbouring layers. The distorted crystal model can be thought of as a local structure, which is broadened by thermally induced CWs.

Subsequently, Regan *et al* [104] have used the same experimental approach to extend the measurements on gallium to study the temperature dependence of the surface-induced atomic layering in liquid gallium. The peak in the reflectivity at $q_z \sim 2.4$ Å^{-1}, arising from the surface layering, decreases dramatically in height upon heating from 22 °C to 170 °C, but its width remains constant (see figure 21).

The decrease in amplitude is attributed to the temperature dependence of CW-induced

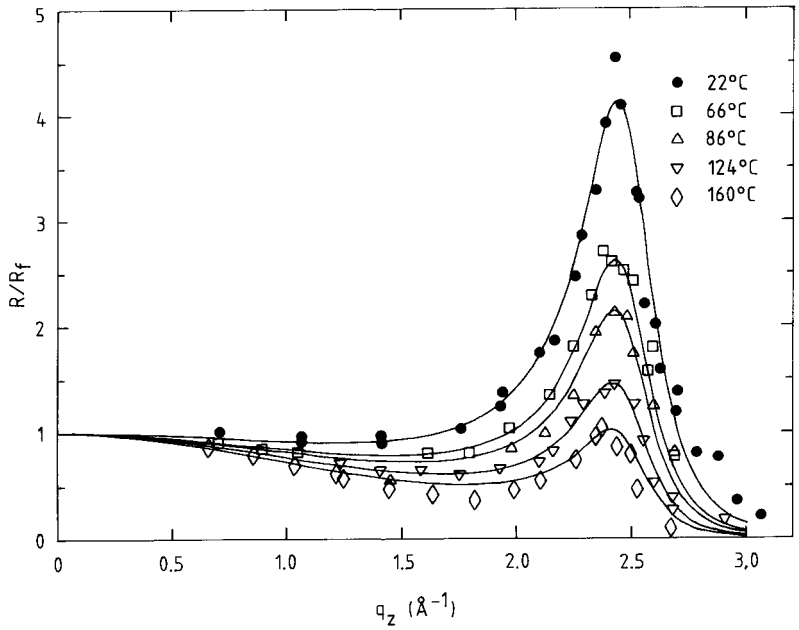

Figure 21. Measured x-ray reflectivity for liquid gallium, normalized to the Fresnel reflectivity, for different temperatures in the range 22–160 °C, the solid curves are calculated curves for the model described in the text (reproduced from [104]).

surface roughness, whereas the constant width indicates that the decay length of the surface layering is independent of temperature. The data were analysed using the same 'distorted crystalline model' as used for liquid gallium and mercury: that is, equally spaced atomic layers with the density distribution broadened by a mean square displacement that increases from the surface into the bulk liquid. To accommodate the thermally induced CWs, the distorted crystalline model is convoluted with a Gaussian $\left(\exp\left(-\sigma_{\mathrm{cw}}^2 z^2\right)\right)$, where σ_{c} is the CW contribution, and this gives good agreement with the expected variation from CW theory.

Finally, Regan *et al* [106] have investigated the effect of oxidation on the structure of the surface of liquid gallium. In the same UHV chamber they have oxidized the clean surface of liquid gallium at room temperature by exposure to increasing doses of oxygen up to a partial oxygen pressure $\sim 2 \times 10^{-4}$ Torr. A gallium oxide film of well defined thickness ~ 5 Å forms (see figure 22), which remains independent of increased oxygen exposure. The well defined oxide layer is inferred from the pronounced and well defined interference fringes that are observed. A quantitative analysis, using the model represented in figure 23, the distorted crystalline model, modified to incorporate the oxide ad-layer, describes well all the data. The oxide thickness and roughness of the air–oxide and oxide–liquid interfaces are invariant with oxygen dosage and temperature. The temperature invariance of the roughness extracted is in marked contrast to that observed for the bare liquid gallium surface, which was roughened by thermally excited CWs. This suggests strongly that the oxide layer provides rigidity to the liquid surface, and is probably solid. Attempts to confirm this with grazing incidence x-ray diffraction measurements have not yet been successful.

Magnussen *et al* [107] have used the same experimental approach to study the specular reflectivity from the surface of liquid mercury up to a q_z of 2.5 Å^{-1}, which is somewhat less experimentally demanding than the surface of liquid gallium. Measurements showed that in

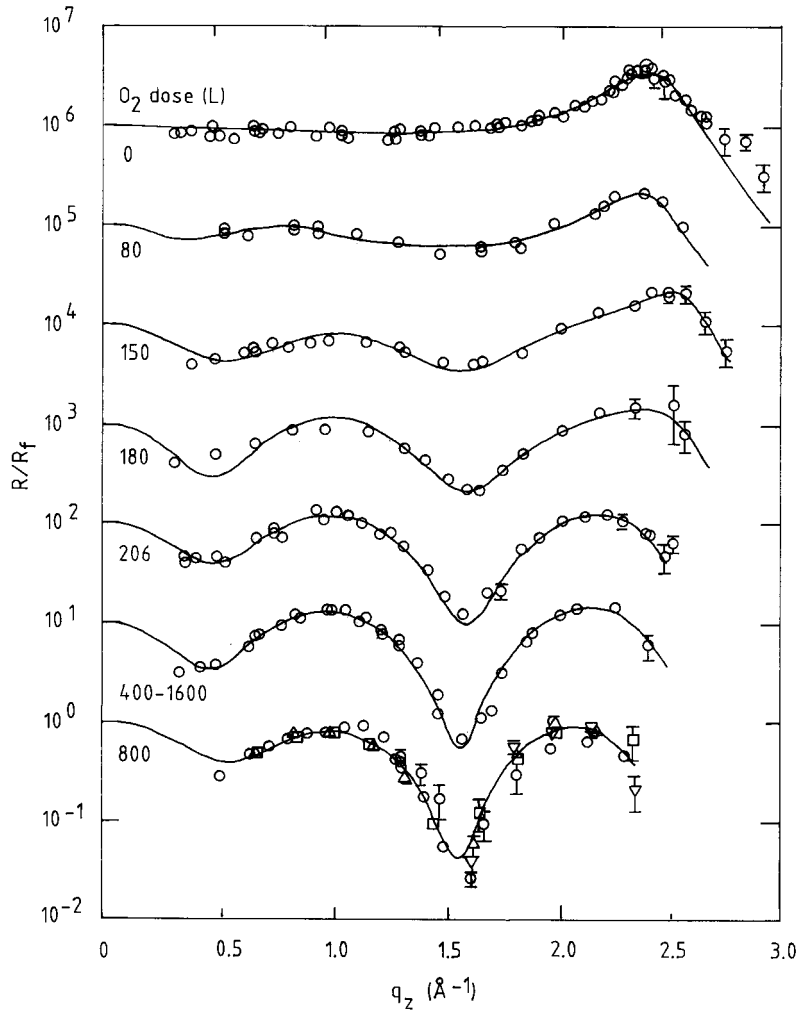

Figure 22. Measured x-ray reflectivity for liquid gallium, normalized to the Fresnel reflectivity, exposed to increasing amounts of oxygen. The solid curves are calculated curves for the distorted crystal model described in the text (reproduced from [106]).

a hydrogen environment the surface was stable and the measured reflectivity reproducible for more than 24 h. The data at high q_z, similar to that for liquid gallium, showed a pronounced peak, and again confirm the existence of surface layering (see figure 24).

Subsequently, DiMasi *et al* [108] measured the temperature dependence of the surface layering in the temperature range -36 to $+25\,^{\circ}$C. The surface structure was described by a layered density profile (see figure 24) convolved with a thermal roughness, σ. The layering had a spacing of 2.72 Å and a decay length of <5 Å. There are some notable differences between the observations for mercury and liquid gallium. For mercury, σ is found to increase faster with temperature than the $T^{\frac{1}{2}}$ predicted by CW theory, in contrast to liquid gallium, and this must arise from a temperature-dependent component in addition to the CW roughening. A direct comparison of the data for mercury and gallium show some qualitative differences at lower q_z, which can be attributed to fundamental differences in the surface structure. In

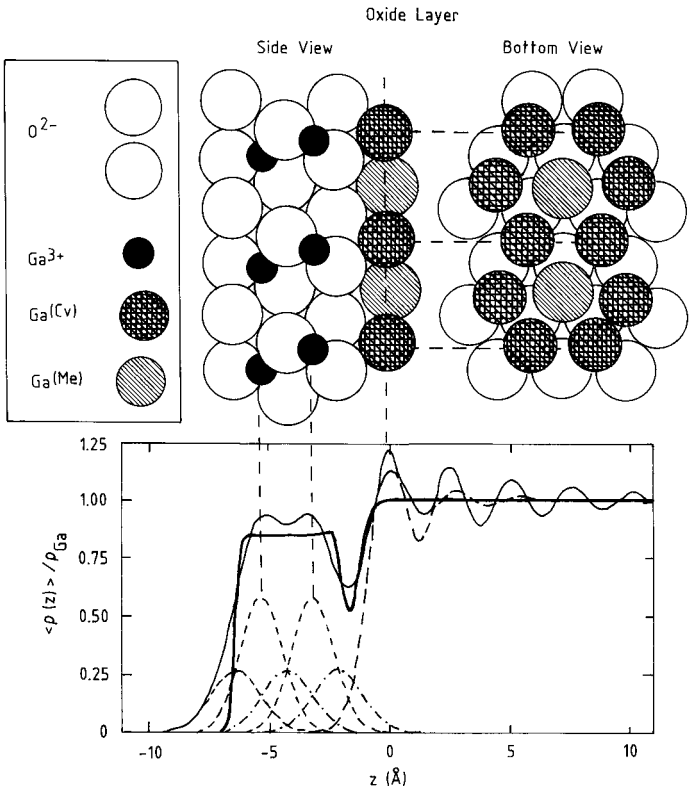

Figure 23. Model of gallium surface, showing proposed atomic arrangement of oxide layer, and corresponding electron density profiles (reproduced from [106]).

particular, for mercury the first layer at the surface is more expanded.

Pershan and co-workers has demonstrated unambiguously, using specular x-ray reflectivity, surface-induced layering. The temperature dependence of the layering shows some differences, and suggests that details of the interaction, such as the degree of covalency, affect the surface structure. Indium is a metal which is almost a free-electron metal, in contrast to gallium which is considerably more covalent. Tostmann *et al* [109] have used x-ray reflectivity and off-specular diffuse scattering to measure the surface of liquid indium close to its melting point, and provided the opportunity for a direct comparison with the results for gallium. In the specular reflectivity a broad peak at a q_z of 2.2 Å^{-1}, similar to that observed for gallium and mercury, is measured. A decay length of 3.5 Å is obtained, shorter than the 5.5 Å obtained for gallium. The off-specular diffuse scattering (see figure 25) is described by the same model, the convolution of the surface structure factor and thermally excited CWs, with no additionally adjustable parameters. Exposure of the liquid indium to oxygen produces no oxide monolayer, unlike the film formed in liquid gallium. The absence of any additional diffuse scattering, beyond that predicted for thermally excited CWs, suggests that the liquid–vapour interface is homogeneous in a direction parallel to the surface, at least on the length scale probed in these measurements. The greater correlation length associated with the surface layering for liquid gallium is an indication of the greater covalency and the directional bonding in the melt.

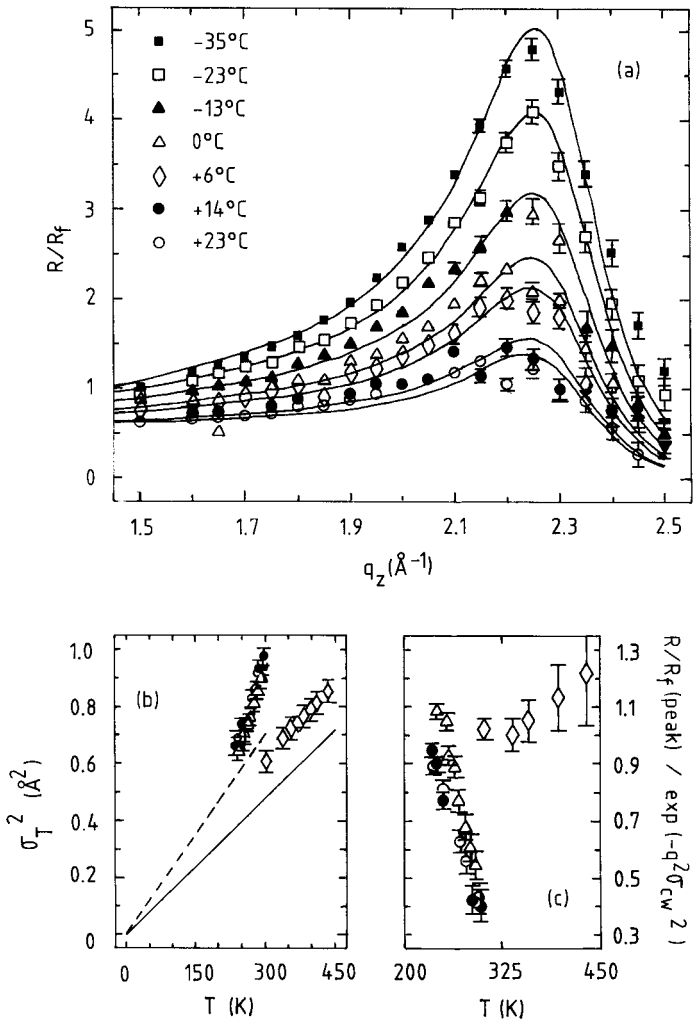

Figure 24. (*a*) X-ray reflectivity for mercury, normalized to the Fresnel reflectivity, for different temperatures in the range −35 to 23 °C. The solid curves are calculated curves for the model described in the text with a variable σ. (*b*) Variation of σ^2 with temperature (△, ●) mercury, (◇) gallium. (*c*) Temperature dependence of $\left(\frac{R}{R_F}\right) / \exp\left(-q_z^2\sigma_{cw}^2\right)$ at the layering peak ($q_z = 2.2$ Å^{-1}) normalized to the melting point (reproduced from [107]).

8. Summary

Recent developments in experimental techniques, such as x-ray reflectivity and x-ray grazing incidence diffraction, have provided the opportunity to confront the predictions of theory and computer simulation on the structure of the surface of liquids. X-ray reflectivity measurements have confirmed the existence of atomic-scale surface layering in liquid metals, and explored the effects of temperature and of oxidation. The opportunity for the study of the increased complexity in alloy surfaces has not been discussed here, but will be an important area of development. The role of CWs and the nature of the intrinsic interfacial width have been

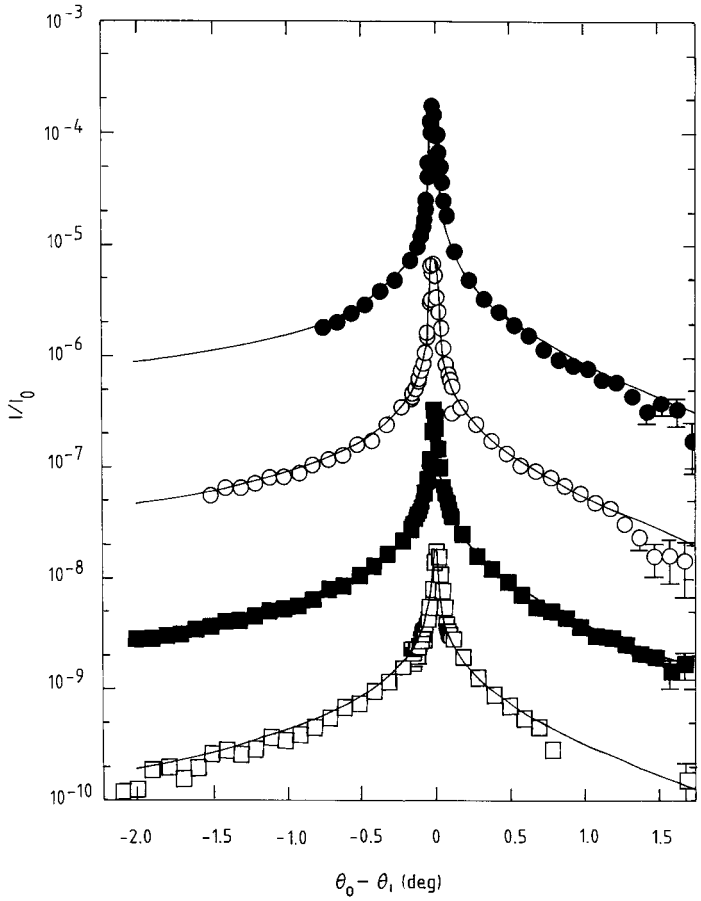

Figure 25. Diffuse scattering as a function of scattering angle, θ_1, for different incoming angles, θ_0, for liquid indium. The solid curves are calculated curves as described in the text (reproduced from [109]).

explored in a range of liquids by x-ray reflectivity, off-specular x-ray surface scattering, ellipsometry and surface quasi-elastic light scattering. The applicability of CW theory and the nature of the upper and lower wavevector cut-offs have been established. Extensions of the application of these experimental methods to the study of more complex molecular fluids, and especially mixtures, are envisaged. The application or development of methods to probe orientational order at the interface in such complex systems should be pursued, and the spectroscopic optical probes, such as second-harmonic generation and sum frequency, are already showing the potential to provide such additional information. X-ray reflectivity, grazing incidence diffraction, and surface tension have recently revealed the phenomenon of surface freezing in liquid alkanes and alcohols, analagous to that observed in liquid crystals. Ellipsometry has been used to probe surface melting or pre-melting, and this remains an area that is still only partially explored. In spite of, or because of, recent theoretical and experimental developments, the study of the structure of the surface of pure liquids remains an exciting and highly relevant area of research.

References

[1] van der Waals J D 1894 *Z. Phys. Chem.* **13** 657
[2] Lord Rayleigh 1892 *Phil. Mag.* **33** 209
[3] Rowlinson J S and Widom B 1982 *Molecular Theory of Capillarity* (Oxford: Oxford University Press)
[4] Croxton C A 1981 *Statistical Mechanics of the Liquid Surface* (New York: Wiley)
[5] Evans R 1979 *Adv. Phys.* **28** 143
[6] 1981 *Faraday Symposium of the Chemical Society* No 16
[7] Croxton C A (ed) 1986 *Fluid Interfacial Phenomena* (New York: Wiley)
[8] Jamin J 1851 *Ann Phys. Chimie* **31** 165
[9] Gibbs J W 1908 *Scientific Papers* (London: Longmans)
[10] Kirkwood J G and Buff F P 1949 *J. Chem. Phys.* **17** 338
[11] Fowler R H 1937 *Proc. R. Soc.* A **159** 229
[12] Evans R 1990 *Liquids at Interfaces (Les Houches Lectures, Session XLVIII)* ed J Charvolin, J F Joanny and J Zinn Justin (Amsterdam: Elsevier)
[13] Evans R 1981 *Mol. Phys.* **42** 1169
[14] Napiorkowski M and Dietrich S 1993 *Phys. Rev.* E **47** 1836
[15] Mecke K R and Dietrich S 1999 *Phys. Rev.* E **59** 6766
[16] Osborn T R and Croxton C A 1980 *Mol. Phys.* **40** 1489
[17] Osborn T R and Croxton C A 1981 *Phys. Lett.* A **81** 278
[18] Evans R 1994 *Bunsenges. Phys. Chem.* **98** 345
[19] Dietrich S 1996 *J. Phys.: Condens. Matter* **8** 9127
[20] Gokelmann B, Hasse A and Dietrich S 1996 *Phys. Rev.* E **53** 3456
[21] Thompson S M, Gubbins K E and Haile J M 1981 *J. Chem. Phys.* **75** 1325
[22] Thompson S M and Gubbins G E 1981 *J. Chem. Phys.* **74** 6467
[23] Gubbins K E and Thompson S M 1981 *Faraday Symposium of the Chemical Society* No 16
[24] Shing K S and Gubbins K E 1982 *Mol. Phys.* **45** 129
[25] Frodl P and Dietrich S 1992 *Phys. Rev.* A **45** 7330
[26] Frodl P and Dietrich S 1993 *Phys. Rev.* E **48** 3741
[27] Frodl P, Groh B and Dietrich S 1994 *Ber Bunseng. Phys. Chem.* **98** 503
[28] Croxton C A 1979 *Phys. Lett.* A **74** 325
[29] Croxton C A 1981 *Physica* A **106** 239
[30] Groh B, Evans R and Dietrich S 1998 *Phys. Rev.* E **57** 6944
[31] Evans R and Slukin T J 1980 *Solid State Phys.* **13** L75
[32] D'Evelyn M P and Rice S A 1983 *J. Chem. Phys.* **78** 5225
[33] D'Evelyn M P and Rice S A 1981 *Faraday Symposium of the Chemical Society* No 16
[34] D'Evelyn M P and Rice S A 1981 *Phys. Rev. Lett.* **47** 1844
[35] Chekmarev D, Zhao M and Rice S A 1998 *J. Chem. Phys.* **109** 768
[36] Chekmarev D S, Zhao M and Rice S A 1999 *Phys. Rev.* E **59** 499
[37] Beaglehole D 1983 *J. Phys. Coll.* C10 44 C10
[38] Meunier J 1987 *J. Phys.* **48** 1819
[39] Meunier J 1996 *Physica* A **280** 27
[40] Langevin D and Meunier J 1983 *J. Phys. C: Solid State Phys.* **10** 44
[41] Mazur E and Chung D S 1987 *Physica* A **147** 387
[42] Earnshaw J C and McGiven R C 1987 *J. Phys. D: Appl. Phys.* **20** 82
[43] Earnshaw J C 1986 *Fluid Interfacial Phenomena* ed C A Croxton (New York: Wiley) p 437
[44] Bain C D 1995 *J. Chem. Soc. Faraday Trans.* **91** 1281
[45] Shen Y R 1989 *Nature* **337** 519
[46] Parratt L G 1954 *Phys. Rev.* **95** 359
[47] Als Nielsen J 1985 *Z. Phys. B: Condens. Matt.* **61** 411
[48] Als Nielsen J and Pershan P S 1983 *Nucl. Instrum. Methods* **208** 545
[49] Pershan P S 1994 *J. Phys.: Condens. Matter* A **6** 37
[50] Sinha S K 1995 *Curr. Opin.* **1** 645
[51] Daillant J 2000 *Curr. Sci.* **71** 1496
[52] Thomas R K and Penfold J 1990 *J. Phys.: Condens. Matter* **1** 1396
[53] Lu J R, Thomas R K and Penfold J 2000 *Adv. Colloid Interface Sci.* **84** 143
[54] Born M and Wolf E 1993 *Principles of Optics* (Oxford: Pergamon)
[55] Honing D and Mobius D 1991 *J. Phys. Chem.* **95** 4590

[56] Jakeman E 1974 *Photon Correlation Light Scattering Spectroscopy* ed H Z Cummins and E R Pike (New York: Plenum) p 75
[57] Pershan P S 1993 *Physica* A **200** 50
[58] Russell T P 1990 *Mater. Sci. Rep.* **5** 171
[59] Pershan P S 1994 *Phys. Rev.* E **50** 2369
[60] Pershan P S 1994 *J. Phys.: Condens. Matter* A **6** 37
[61] Lu J R, Lee E M and Thomas R K 1996 *Acta Crystallogr.* A **11** 52
[62] Schlossman M L, Synal D, Guan Y, Meron M, Shea-McCarthy G, Huang Z, Acero A, Williams S M, Rice S A and Jones Viccaro P 1997 *Rev. Sci. Instrum.* **68** 4372
[63] Sinha S K, Sirota E B, Garoff S and Stanley H E 1988 *Phys. Rev.* B **38** 2297
[64] Pynn R 1992 *Phys. Rev.* B **46** 7953
[65] Sinha S K 1995 *Mater. Res. Soc. Symp. Proc.* **376** 175
[66] Holy V, Kubena J, Van der Hoogenhof and Vavra I 1995 *Appl. Phys.* A **60** 93
[67] Yoneda Y 1963 *Phys. Rev.* **131** 2010
[68] Fradin C *et al* 1996 *Physica* B **248** 310
[69] Beaglehole D 1979 *Phys. Rev. Lett.* **43** 2016
[70] Beaglehole D 1980 *Physica* B **100** 163
[71] Beaglehole D 1987 *Phys. Rev. Lett.* **58** 1434
[72] Buff F P, Lovett R A and Stillinger F H 1965 *Phys. Rev. Lett.* **15** 621
[73] Beysens D and Meunier J 1988 *Phys. Rev. Lett.* **61** 2001
[74] Braslau A, Pershan P S, Swislow G, Ocko B M and Als-Nielsen J 1988 *Phys. Rev.* A **38** 2457
[75] Stringari S and Treiner J 1987 *Phys. Rev.* B **36** 8369
[76] Lurio L B, Rabedeau T A, Pershan P S and Silvera I F 1991 *Physica* B **169** 507
[77] Lurio L B, Rabedeau T A, Pershan P S, Silvera I F, Deutsch M, Kosowsky S D and Ocko M B 1992 *Phys. Rev. Lett.* **68** 2628
[78] Lurio L B, Rabedeau T A, Pershan P S, Silvera I F, Deutsch M, Kosowsky S D and Ocko B M 1993 *Phys. Rev.* B **48** 9644
[79] Braslau A, Deutsch M, Pershan P S, Weiss A H, Als-Nielsen J and Bohr J 1985 *Phys. Rev. Lett.* **54** 114
[80] Beaglehole D 1987 *J. Phys. Chem.* **91** 5091
[81] Beaglehole D 1993 *Physica* A **200** 696
[82] Schwartz D K, Schlossman M L, Kawamoto E H, Kellogg G J, Pershan P S and Ocko B M 1990 *Phys. Rev.* A **41** 5687
[83] Townsend R M and Rice S A 1991 *J. Chem. Phys.* **94** 2207
[84] Sinha S K 1996 *Physica* A **224** 140
[85] Beaglehole D and Wilson P 1993 *J. Phys. Chem.* **97** 11053
[86] Beaglehole D and Wilson P 1994 *J. Phys. Chem.* **98** 8096
[87] Elbaum M, Lipson S G and Dash J G 1993 *J. Crystal Growth* **129** 491
[88] Wu X Z, Ocko B M, Sirota E B, Sinha S K, Deutsch M, Cao B H and Kim M W 1993 *Science* **261** 1018
[89] Gang H, Patel J, Wu Z X, Deutsch M, Gang O, Ocko B M and Sirota E B 1998 *Europhys. Lett.* **43** 314
[90] Pfohl T, Beaglehole D and Riegler H 1996 *Chem. Phys. Lett.* **260** 82
[91] Wu Z X, Sirota E B, Sinha S K, Ocko B M and Deutsch M 1993 *Phys. Rev. Lett.* **70** 958
[92] Wu Z X, Ocko B M, Sirota E B, Sinha S K and Deutsch M 1993 *Physica* A **200** 751
[93] Ocko B M, Wu Z X, Sirota E B, Sinha S K, Gang O and Deutsch M 1997 *Phys. Rev.* E **55** 3164
[94] Deutsch M, Wu Z X, Sirota E B, Sinha S K, Ocko B M and Magnussen O M 1995 *Europhys. Lett.* **30** 283
[95] Gang O, Wu Z X, Ocko B M, Sirota E B and Deutsch M 1998 *Phys. Rev.* E **58** 6086
[96] Sanyal M K, Sinha S K, Huang K G and Ocko B M 1991 *Phys. Rev. Lett.* **66** 628
[97] Ocko B M, Wu Z X, Sirota E B, Sinha S K and Deutsch M 1994 *Phys. Rev. Lett.* **72** 242
[98] Chu B and Rice S A 1978 *J. Chem. Phys.* **68** 5558
[99] Lang N D 1973 *Solid State Phys.* **28** 224
[100] Kawamoto E H, Lee S, Pershan P S, Deutsch M, Maskil N and Ocko B M 1993 *Phys. Rev.* B **47** 6847
[101] Regan M J, Kawamoto E H, Lee S, Pershan P S, Maskil N, Deutsch M, Magnussen O M, Ocko B M and Berman L E 1995 *Phys. Rev. Lett.* **75** 2498
[102] Regan M J, Kawamoto E H, Lee S, Pershan P S, Maskil N, Deutsch M, Magnussen O M, Ocko B M and Berman L E 1996 *J. Non-Cryst. Solids* **205-7** 762
[103] Magnussen O M, Regan M J, Kawamoto E H, Ocko B M, Pershan P S, Maskil N, Deutsch M and Berman L E 1996 *Phys. Rev.* B **54** 9730
[104] Regan M J, Pershan P S, Magnussen O M, Ocko B M, Deutsch M and Berman L E 1996 *Phys. Rev.* B **54** 9730
[105] Regan M J, Pershan P S, Magnussen O M, Ocko B M, Deutsch M and Berman L E 1997 *Phys. Rev.* B **55** 15874

[106] Regan M J, Tostmann H, Pershan P S, Magnussen O M, DiMasi E, Ocko B M and Deutsch M 1997 *Phys. Rev.* B **55** 10786
[107] Magnussen O M, Ocko B M, Regan M J, Penanen K, Pershan P S and Deutsch M 1995 *Phys. Rev. Lett.* **74** 4444
[108] DiMasi E, Tostmann H, Ocko B M, Pershan P S and Deutsch M 1998 *Phys. Rev.* B **58** R13419
[109] Tostmann H, DiMasi E, Pershan P S, Ocko B M, Shpyrko O G and Deutsch M 1999 *Phys. Rev.* B **59** 783